Atomic motions in the $\alpha\beta$-merging region of 1,4-polybutadiene: A molecular dynamics simulation study

A. Narros, A. Arbe, F. Alvarez, J. Colmenero, and D. Richter

Citation: The Journal of Chemical Physics **128**, 224905 (2008); doi: 10.1063/1.2937733
View online: https://doi.org/10.1063/1.2937733
View Table of Contents: http://aip.scitation.org/toc/jcp/128/22
Published by the American Institute of Physics

Atomic motions in the $\alpha\beta$-merging region of 1,4-polybutadiene: A molecular dynamics simulation study

A. Narros,[1] A. Arbe,[2,a)] F. Alvarez,[1,2] J. Colmenero,[1,2,3] and D. Richter[4]
[1]*Departamento de Física de Materiales UPV/EHU, Apartado 1072, 20080 San Sebastián, Spain*
[2]*Centro de Física de Materiales (CSIC-UPV/EHU), Apartado 1072, 20080 San Sebastián, Spain*
[3]*Donostia International Physics Center, Paseo Manuel de Lardizabal 4, 20018 San Sebastián, Spain*
[4]*Institut für Festkörperforschung, Forschungszentrum Jülich GmbH, D-52425 Jülich, Germany*

(Received 22 January 2008; accepted 7 May 2008; published online 11 June 2008)

We present fully atomistic molecular dynamics simulations on 1,4-polybutadiene in a wide temperature range from 200 to 280 K, i.e., in the region where the α- and β-relaxations merge and above. A big computational effort has been performed—especially for the lowest temperatures investigated—to extend the simulation runs to very long times (up to 1 μs for 200 K). The simulated sample has been carefully validated by using previous neutron scattering data on the real sample with similar microstructure. Inspecting the trajectories of the different hydrogens in real space, we have observed a heterogeneous dynamical behavior (each kind of hydrogen moves in a different way) with signatures of combined hopping and diffusive motions in the whole range investigated. The application of a previously proposed model [Colmenero *et al.*, Europhys. Lett. **71**, 262 (2005)] is successful and a characterization of the local motions and diffusion is possible. The comparison of our results to those reported in the literature provides a consistent scenario for polybutadiene dynamics and puts into a context the different experimental observations. We also discuss the impact of the hopping processes on the observation and interpretation of experimentally accessible magnitudes and the origin of the deviations from Gaussian behavior in this system.
 [DOI: 10.1063/1.2937733]

I. INTRODUCTION

1,4-polybutadiene (1,4-PB) is considered as an archetypal polymer due to its lack of side groups and amorphous character. Therefore, it has been taken as a model system to investigate glassy and supercooled liquid dynamics and, for example, to check theoretical predictions such as those of the mode coupling theory (MCT) for the glass transition.

This polymer has indeed been deeply investigated by diverse techniques. From an experimental point of view, there is a large number of studies dealing with relaxation techniques, e.g., dielectric spectroscopy (DS),[1–4] mechanical spectroscopy,[5,6] or NMR,[4] and many investigations rest on scattering techniques, including light scattering,[7,8] inelastic x-ray scattering,[9] and neutron scattering.[2,3,9–23] Moreover, 1,4-PB is one of the most simulated polymers both with united atom and with fully atomistic models (see, e.g., Refs. 22–36). The compilation of all these studies revealed rather complex dynamical properties of this "in principle simple" polymer close and above its glass transition temperature T_g($T_g \approx 180$ K). This complexity can be appreciated in Fig. 1. As predicted by the MCT,[37] the structural relaxation which is directly observed through the decay of intermolecular correlations at the peak of the dynamic structure factor[10] follows the temperature dependence of the viscosity (i.e., the structural relaxation time τ_s is proportional to η/T). This last was deduced from measurements on the monomeric friction coefficient ξ.[5] On the other hand, the dielectric spectra reveal the genuine structural relaxation only if the strong contribution of the Johari–Goldstein β-process is properly taken into account in the analysis procedure.[3] This process has a characteristic time at T_g of ≈ 10 μs.[2] Aiming to unveil the molecular origin of this secondary relaxation, coherent neutron scattering experiments by neutron spin echo (NSE) were performed at the second maximum of the dynamic structure factor, which origin is of intramolecular nature.[2,3] The decay of these correlations showed a timescale with similar activation energy as the DS β-process, but was more than two orders of magnitude faster. Later depolarized light scattering works[7,8] focused on unraveling this discrepancy and reported an apparently additional dynamical process even faster than that observed by NSE. A recent NMR and DS study[4] has identified a process deep in the glassy state. Extrapolating its timescale, this further process appears to match that observed by light scattering[8] well in the supercooled regime.

In view of the puzzling situation, molecular dynamics (MD) simulations are important, in order to find a consistent interpretation of the dynamical processes taking place in 1,4-PB close and above the glass transition. In particular, the temperature region where the α (structural) relaxation and the Johari–Goldstein β-process (≈ 220 K) merge is extremely interesting due to the variety of identified dynamical processes. However, such MD studies at relatively low temperatures are associated with long structural relaxation times and therefore require long equilibration runs. On the other hand, fully atomistic simulations are needed since only they

a)Electronic mail: waparmea@sc.ehu.es.

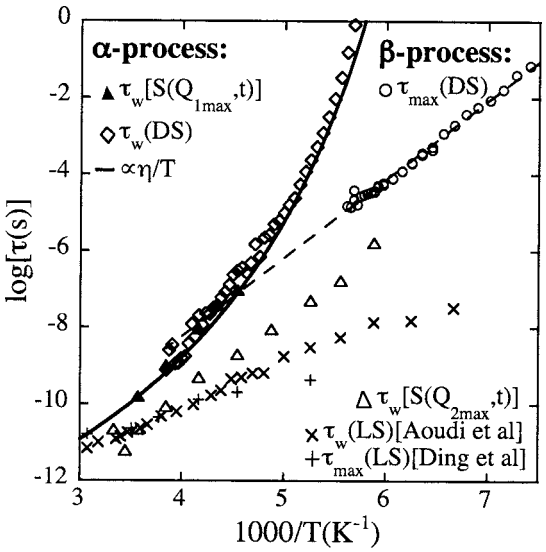

FIG. 1. Relaxation map compiled for 1,4-PB: DS results on the α (diamonds) and β (circles) processes (Refs. 2 and 3), NSE results on the dynamic structure factor at its first maximum (full triangles) (Ref. 10) and second maximum (empty triangles) (Refs. 2 and 3), and light scattering results [crosses (Ref. 7) and pluses (Ref. 8)]. The solid line is based on measurements of the monomeric friction coefficient (Ref. 5), and the dashed line is an Arrhenius fit of the β-process.

allow a more detailed insight in the particular motions taking place in systems such as 1,4-PB, which are characterized by a relatively rich microstructure.

With these ideas in mind, we have performed fully atomistic MD simulations on 1,4-PB in a wide temperature range from 200 to 280 K. The simulated polymer has the same microstructure as the real samples which were synthesized by anionic polymerization. This allows a careful and critical validation by direct comparison to experimental results obtained by neutron scattering. Results at 200 K involving simulation runs up to 300 ns were recently published.[23] There, a real space analysis of the simulation results allowed an identification of hopping and diffusion processes and we proposed a phenomenological model based on the simultaneous occurrence of both kinds of motion. In this work, we have extended this study toward longer times with a simulation run of 1 μs and toward higher temperatures, with the goal to address the question of how the two processes are combining and how they develop with varying temperature. As a first step, using previous neutron scattering data on 1,4-PB covering more than four decades in time ($\approx$0.1 ps– $\approx$5 ns), we have carefully validated our simulated sample. Inspecting the trajectories of the different hydrogens in real space, we have observed a heterogeneous dynamical behavior (each kind of hydrogen moves in a different way) with signatures of combined hopping and diffusive motions in the whole range investigated. The application of the previously proposed model[23] is successful and a characterization of the local motions and diffusion is possible. We have also performed a careful comparison of our model with literature results on the there reported processes in order to get a consistent scenario and put into a context the different experimental observations. We also discuss the impact of the hopping processes on the observation and interpretation of experimentally accessible magnitudes and the origin of the deviations from Gaussian behavior in this system. Finally, the applicability of MCT to 1,4-PB is shortly discussed in relation to Ref. 38.

II. MOLECULAR DYNAMICS SIMULATIONS

The simulations were carried out by using the INSIGHT (Insight II 4.0.0 P version) and the DISCOVER-3 module from Molecular Simulations Inc. (now Accelrys) with the polymer consortium force field (PCFF). Most parameters of this field were derived based on *ab initio* data using a least-squares-fit technique developed by Hagler and co-workers. More information about the force fields, including the complete analytical expression for the functional form, can be found in Refs. 39 and 40. The simulations were divided in two parts: A first model system was built by means of the amorphous cell protocol, which was originally proposed by Theodorou and Suter.[41,42] In this procedure, the model system is a cubic cell with three-dimensional periodic boundaries, filled with chain segments at a density corresponding to the experimental value for the polymer. The entire contents of the cube are formed from a single "parent chain." The cube can be considered as part of an infinite medium, consisting of displaced images of the same chain. Thus, within the cube, we can find polymer segments belonging to the parent chain surrounded by segments corresponding to images of the chain. These last, effectively, can be considered as belonging to different chains. Therefore, we note that within such simulated cell both kinds of correlations, of inter- and intrachain nature, are present. In this work, a cubic cell containing one polymer chain of 130 monomer units of polybutadiene, 1,4-PB [with a chemical composition of 7% of 1,2-PB (vinyl) units, 53% of 1,4-PB-*trans* and 40% of 1,4-PB-*cis*] was constructed at 280 K in a cell under periodic boundary conditions. The density was achieved in running *NPT* dynamics (keeping constant the number of atoms, the pressure, and the temperature in the cell) on a system where the starting value of the unknown density was estimated to be 0.9 g/cm^3. However, this value was an overestimation. Applying subsequently a trial and error procedure where both *NPT* dynamics (to obtain density estimates) and *NVT* dynamics (keeping constant the number of atoms, the cell size and the temperature of the sample) were combined, the data were collected and compared to actual experimental values. The value 0.835 g/cm^3 leading to a cell side of 24.0949 Å was found to reasonably describe the neutron scattering results (see below). In order to perform this comparison to the experimental values, standard minimization procedures (Polak–Ribiere conjugate gradients method) were followed minimizing the so obtained energy structure. The subsequent dynamics with the fixed value for the density was run for t_{eq}=1 ns in order to equilibrate the sample. This time is long enough to assure local structural equilibration of the sample, since at this temperature the structural relaxation time τ_s is $\approx$0.2 ns (see later). The system obtained in this way was used as a starting point for collecting data every 0.01 ps during a MD run of 1 ns. As integration method, we have used the velocity-Verlet algorithm with a time step of 1 fs. The simulations were carried

TABLE I. Density, cell side, and duration of the maximum time acquisition runs for the different temperatures simulated.

T (K)	ρ (g/cm^3)	ℓ (Å)	t_{ac} (ns)
200	0.8789	23.6865	1000
220	0.8677	23.7833	200
230	0.8625	23.8347	100
240	0.8567	23.8897	40
260	0.8458	23.9919	20
280	0.8350	24.0949	20

out in the *NVT* ensemble. However, for temperature control instead of a real temperature-bath coupling (Nose–Hoover or Berendsen thermostats, for instance) we have followed a rather crude velocity scaling procedure but with a wide temperature window of 10 K. Under these conditions, greater temperature fluctuations are allowed but the trajectory is disturbed less. In fact, we have checked that by following this simple procedure we obtain results similar to those obtained with a *NVE* ensemble (by keeping constant the sample total energy instead of its temperature), which has the proper Newtonian dynamics. After the first data collecting 1 ns MD run, two successive runs of 2 and 20 ns were carried out, collecting data every 0.05 and 0.5 ps, respectively. Nearly indistinguishable results were obtained from the different simulation runs.

The so obtained system was used to yield corresponding cells at different lower temperatures, namely, 260, 240, 230, 220, and 200 K. In order to do this, *NPT* simulation runs of at least 3 ns were used to readapt the system to each new temperature, step by step, thus allowing the size of the system to rearrange itself so it could accommodate to the new density at each temperature. In this way, we got the values displayed in Table I for the cell size and density. Subsequent *NVT* runs were performed for equilibration at each temperature before collecting data for analysis. The length of these equilibration runs was as high as 100 ns for the lower temperatures. Afterwards *NVT* runs were performed to collect data (duration of the acquisition time t_{ac} displayed in Table I) in the same way as above described for 280 K.

III. CORRELATION FUNCTIONS AND NEUTRON SCATTERING CROSS SECTIONS

Starting from the atomic trajectories in space, i.e., the time-dependent position of the ith atom $\vec{r}_i(t)$ for $i=1,\ldots,N$ (N: Number of atoms in the sample), the self-part of the van Hove correlation function $G_s(\vec{r},t)$ may be calculated directly. Thereby $G_s(\vec{r},t)$ is the probability to find an atom at time t at a position $\vec{r}$ if it was at $\vec{r}=0$ for $t=0$:

$$G_s(\vec{r},t)=\frac{1}{N}\left\langle \sum_{i=1}^{N}\delta[\vec{r}-(\vec{r}_i(t)-\vec{r}_i(0))]\right\rangle. \tag{1}$$

The brackets denote the ensemble average. The sum in Eq. (1) may be also restricted to a subset of atoms of kind α in the sample (e.g., α: Hydrogen, Carbon, etc.).

The Fourier transformation of $G_s(\vec{r},t)$ into the reciprocal space yields the intermediate scattering function $F_s(\vec{Q},t)$,

$$F_s(\vec{Q},t)=\int G_s(\vec{r},t)\exp(i\vec{Q}\vec{r})d\vec{r}. \tag{2}$$

Finally, the so-called incoherent scattering function $S_s(\vec{Q},\omega)$ is obtained by subsequent Fourier transformation into the frequency domain:

$$S_s(\vec{Q},\omega)=\frac{1}{2\pi\hbar}\int F_s(\vec{Q},t)\exp(-i\omega t)dt. \tag{3}$$

For some simple cases—free nuclei in a gas, harmonic crystals, simple diffusion at long times—$G_s(\vec{r},t)$ is a Gaussian function;[43] in an isotropic system this implies

$$G_s^{\text{Gauss}}(r,t)=\left[\frac{\alpha(t)}{\pi}\right]^{3/2}\exp[-\alpha(t)r^2]. \tag{4}$$

In the Gaussian approximation, the even moments of $G_s(r,t)$

$$\langle r^{2n}\rangle=\int_0^\infty r^{2n}G_s(r,t)4\pi r^2dr \tag{5}$$

can be straightforwardly calculated. For instance, the mean squared displacement of the atom $\langle r^2(t)\rangle$ is given by $\langle r^2(t)\rangle=3/[2\alpha(t)]$. It is also easy to realize that then $F_s(Q,t)$ is also Gaussian in Q and entirely determined by $\langle r^2(t)\rangle$:

$$F_s^{\text{Gauss}}(Q,t)=\exp\left[-\frac{\langle r^2(t)\rangle}{6}Q^2\right]. \tag{6}$$

In more general cases, deviations of $G_s(r,t)$ from the Gaussian form [Eqs. (4) and (6)] may be expected. The intermediate scattering function $F_s(Q,t)$ can then be expressed in terms of its expansion in Q^2 (see, e.g., Ref. 18),

$$F_s(Q,t)=\exp\left[-\frac{\langle r^2(t)\rangle}{6}Q^2+\frac{\alpha_2(t)\langle r^2(t)\rangle^2}{72}Q^4+\cdots\right], \tag{7}$$

where the second order non-Gaussian parameter $\alpha_2(t)$ giving the leading correction can be obtained from the moments of $G_s(r,t)$:[44]

$$\alpha_2(t)=\frac{3}{5}\frac{\langle r^4(t)\rangle}{\langle r^2(t)\rangle}-1. \tag{8}$$

Obviously, in the Gaussian case, $\alpha_2(t)=0$.

Until here, we have dealt with correlation functions involving a single particle. However, the structural information of the system involves relative positions of different atoms. The van Hove correlation function $G(\vec{r},t)$ relates positions of pairs of atoms at different times,

$$G(\vec{r},t)=\frac{1}{N}\left\langle \sum_{i,j=1}^{N}\delta[\vec{r}-(\vec{r}_i(t)-\vec{r}_j(0))]\right\rangle. \tag{9}$$

The Fourier transform of this correlation function in the reciprocal space is the dynamic structure factor $S(Q,t)$ [obtained in an equivalent way as in Eq. (2)]. The well-known static structure factor $S(Q)$ is just the value of $S(Q,t=0)$. In analogy with Eq. (3), the Fourier transformation of the dynamic structure factor into the frequency domain delivers the scattering function $S(Q,\omega)$.

All the above correlation functions and related magnitudes can easily be calculated from the MD-simulation tra-

TABLE II. Incoherent and coherent cross sections and coherent scattering lengths of the isotopes involved in this study.

Nucleus	σ_{inc} (barns)	σ_{coh} (barns)	$\bar{b}$ (fm)
H	80.27	1.7583	−3.7406
D	2.05	5.592	6.671
C	0	5.559	6.6511

jectories. Neutron scattering offers the opportunity to investigate some of these correlation functions on real samples (see Refs. 43 and 45–47). These experiments assess the double differential cross section, i.e., the fraction of scattered neutrons into a solid angle between Ω and $\Omega+d\Omega$ which have experienced an energy transfer $\hbar\omega$. The modulus of the momentum transfer, Q, is determined by $Q=4\pi\sin(\theta/2)/\lambda$, where θ is the scattering angle and λ the wavelength of the incoming neutrons.

The scattering may be either incoherent or coherent. Incoherent scattering relates to single-particle motions, i.e., it reveals the incoherent scattering function $S_s(Q,\omega)$. Coherent scattering is determined by the scattering function $S(Q,\omega)$ reflecting collective dynamics. Each kind of isotope α interacts in a different way with neutrons, displaying a different scattering length b_α. The different averages over these scattering lengths lead to the coherent ($\sigma_{coh}=4\pi\bar{b}^2$) and incoherent [$\sigma_{inc}=4\pi(\langle b_\alpha^2\rangle-\langle\bar{b}_\alpha\rangle^2)$] cross sections. The values of σ_{inc}, σ_{coh}, and $\bar{b}$ are shown in Table II for the three types of nuclei involved in this study. Due to the large value of σ_{inc}^H, in a fully protonated sample, the measured intensity is clearly dominated by the incoherent scattering of hydrogen $S_s^H(Q,\omega)$. On the contrary, in a fully deuterated sample, the incoherent intensity is strongly reduced; as the coherent scattering lengths of C and D are practically the same, the scattered intensity reveals directly the coherent scattering function with all atomic pairs equally weighted, i.e., $S(Q,\omega)$ as defined above, involving all nuclei in the sample.

Since experimentally the spatial information is obtained through the Q-dependence of the intensities, only the reciprocal space is accessible and the functions in real space [e.g., $G_s(r,t)$, $\langle r^2(t)\rangle$, $\alpha_2(t)$, $G(r,t)$] cannot be directly addressed. On the other hand, most of the spectrometers (time of flight, backscattering, etc.) are based on direct measurements of neutron energy changes, thereby delivering the scattering functions $S_s(Q,\omega)$ and $S(Q,\omega)$ in the frequency domain. The evolution of the accessible correlation functions in the time domain [i.e., $F_s^H(Q,t)$ or $S(Q,t)$] can only be followed by a special technique known as NSE.[48]

IV. VALIDATION

A necessary step prior to the exploitation of MD simulations is their validation by direct comparison to experimentally accessible magnitudes. In a previous work,[22] we have shown that the structural properties of the cell correspond well to those of the real sample. The short range order of the polymer as revealed by neutron diffraction on deuterated 1,4-PB (1,4-PBd) and protonated 1,4-PB (1,4-PBh) (accessing thus the full structure factor and a partial structure factor)

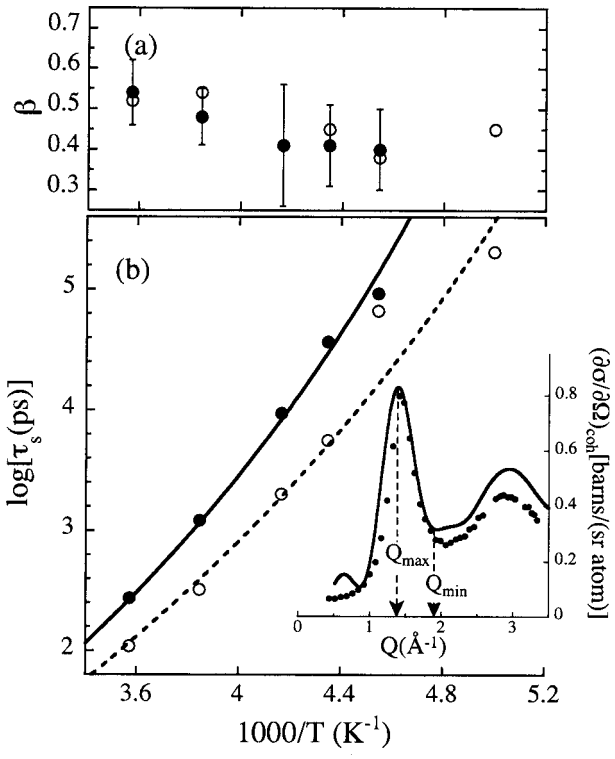

FIG. 2. Temperature dependence of the KWW parameters describing the decay of the structure factor of 1,4-PB at 1.5 Å^{-1} and $t\geqslant 2$ ps: (a) Shape parameter and (b) characteristic time. Full symbols correspond to experimental (NSE) data (Refs. 3 and 10) and empty symbols to simulation data. The solid line shows the temperature dependence expected from viscosity measurements (Ref. 5). The dotted line represents the same curve with a shift in the Vogel–Fulcher temperature of −15 K. Inset: Structure factor measured on a fully deuterated sample (Ref. 22) (points) and calculated from the simulations (line) at 200 K.

is very well reproduced by the simulated cell. As an example, the inset of Fig. 2 displays the good agreement for the static structure factor $S(Q)$ at 280 K. Also the temperature dependence of the diffraction patterns is fairly captured.[22]

Now moving to the dynamical features, crucial tests can be performed by considering results corresponding to both protonated and deuterated samples, since then the reproducibility of both single-particle motions (those of the hydrogens) and collective dynamics is checked.

First we consider the NSE results (covering times from $\approx$5 ps to $\approx$5 ns) on the direct observation of the structural relaxation. This is achieved by studying the normalized dynamic structure factor at its first peak $S(Q_{max},t)/S(Q_{max})$. As shown in the inset of Fig. 2, Q_{max} is located at about 1.4 Å^{-1} at high temperatures. A direct comparison of the NSE results obtained on the deuterated sample at $Q=1.48$ Å$^{-1}\approx Q_{max}$ (Refs. 3 and 10) with our simulation data at the same Q-value reveals slightly faster decays for the simulated structure. In order to quantify the difference between both sets of data, we have used the well-known stretched exponential or Kohlrausch–Williams–Watts (KWW) functional form: After the initial microscopic regime ($t\lesssim 2$ ps) leading to a decay of the correlations characterized by the Debye–Waller factor (DWF), the normalized structure factor is described by (see, e.g., Ref. 49)

$$\frac{S(Q_{\max},t)}{S(Q_{\max})} = \mathrm{DWF}\exp\left[-\left(\frac{t}{\tau_s}\right)^{\beta}\right], \tag{10}$$

where β is the stretching exponent and τ_s is the structural relaxation time. We have used Eq.(10) to describe both NSE and simulation data at $Q=1.48$ Å$^{-1}\approx Q_{\max}$ individually for each temperature. We note that this kind of analysis has never been reported for 1,4-PBd NSE data. Due to the limited NSE dynamic window, the determination of the shape parameter β is subject of rather high uncertainties if no assumption is made about the prefactor of the fitting curve.[50] Therefore, in the previous works the time-temperature superposition principle has always been assumed and the data were analyzed by constructing master curves. Figure 2 shows the results here obtained. Within the rather large uncertainties of the NSE shape parameter, the values of β deduced from both techniques are compatible. On the other hand, the timescales are systematically faster for the simulations. As shown in Fig. 2(b), the NSE times can be perfectly described by the temperature dependence proposed in Ref. 10,

$$\tau_s = \frac{A}{T}\exp\left[\frac{B}{(T-T_o)}\right], \tag{11}$$

where B and T_0 are determined from the monomeric friction coefficient ($B=1404.5$ K, $T_0=128$ K).[5] We obtain a value of 7.22 ps K for the prefactor A. Fixing these values of A and B, a rather good description of the simulation structural times is obtained by Eq. (11) with $T_0=113$ K [see Fig. 2(b)]. This means the relaxation times of the simulations and the real sample approximately coincide if we assume a shift in the glass transition temperature of 15 K ($T_g^{\mathrm{MD}}=T_g^{\mathrm{real}}-15$ K).

We now may ask whether such a shift in T_0 is consistent and allows to describe the NSE results on different correlation functions. We have considered, apart from the structure factor at the maximum, the structure factor at the minimum[13] ($Q_{\min}\approx 1.9$ Å^{-1}, see inset in Fig. 2) and the intermediate scattering function of the hydrogen $F_s^{\mathrm{H}}(Q,t)$ measured on the protonated sample.[23] For these functions, Fig. 3 displays the MD-simulation data together with NSE results. The timescales of the experimental data have been shifted toward faster values according to the deduced $\Delta T_0=15$ K. The comparison also involves corrections for bandpass effects which affect the NSE amplitudes. To do this, in Figs. 3(a) and 3(c), we have used the simulation result of the correlation function at 0.2 ps, in the same way as explained for polyisoprene,[51] 1,2-PB,[52] and poly(methyl methacrylate)(PMMA).[53] For the case of the structure factor at the minimum, such criterion delivered slightly overcorrected amplitudes (between 10% and 15% overcorrection). There, we have readjusted the corrections to match the experimental and simulation data. As we can see in Fig. 3, all correlation functions are fairly well reproduced by the MD simulations in this way. Though the coincidence of $S(Q_{\max},t)/S(Q_{\max})$ could seem trivial after the procedure followed for the comparison, the agreement is not evident at all *a priori* for the other correlation functions and the spectral shapes. We remark the overall excellent description regarding the temperature and Q dependencies and the spectral shapes of both correlation functions.

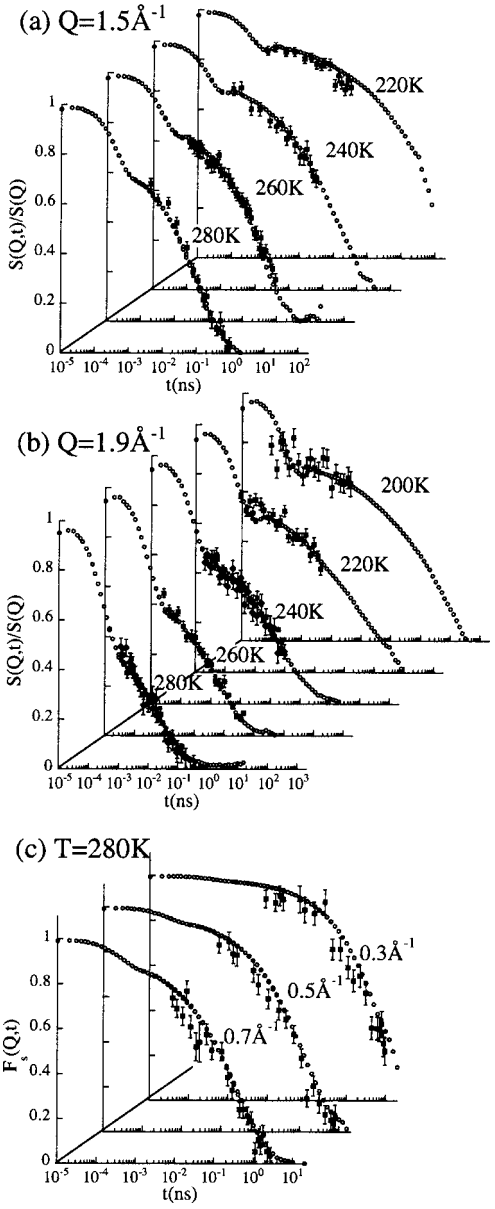

FIG. 3. Comparison between MD-simulation (empty circles) and NSE (full squares) results on 1,4-PB: (a) Dynamic structure factor at 1.5 Å^{-1} (close to the first maximum) and (b) at 1.9 Å^{-1} (close to the first minimum) for the different temperatures indicated. (c) Incoherent scattering function of the hydrogens at 280 K the different Q-values indicated. In all cases, the timescale of the experiments has been shifted assuming a shift of −15 K in T_o.

We also compare the results within the dynamic window accessed by time of flight (covering also the microscopic region around and below 1 ps). Figure 4(a) shows the direct comparison of MD-simulation results and the Fourier transformed data obtained for 1,4-PBh published in Ref. 6. The experimental data are slightly slower than the MD simulations. In Fig. 4(b), we have applied the same shift as in the comparison of the NSE data. In this way, a perfect matching is achieved in the region of the second step of the intermediate scattering function. This result is fully consistent with the NSE comparison. We note, however, that such shift is too large to match the microscopic regimes.

The need of frequency or temperature shifts to match simulated and experimental results has been reported for sev-

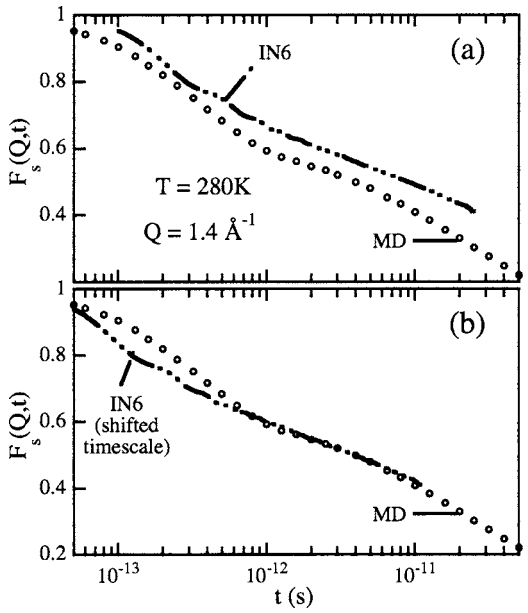

FIG. 4. Comparison between MD-simulation (empty circles) and time of flight (dashed-dotted) results (Ref. 6) on the incoherent scattering function of hydrogen in 1,4-PB at 280 K and $Q=1.4$ Å^{-1}. In panel (b), the timescale of the experiments has been shifted toward faster times in the same way as the NSE results.

eral systems, e.g., orthoterphenyl,[54] PI,[51] or PMMA.[53,55] Apart from small differences in the microstructure or in the density, a possible source for this discrepancy could be that the force field used in the simulations was not perfectly calibrated. For polybutadiene, it has been shown by Smith *et al.*[27] that the timescale of the α-relaxation resulting from the MD simulations is quite sensitive to slight changes of the local intrachain potentials. Our comparison suggests, in fact, that the intramolecular potentials determining the microscopic dynamics are better calibrated than the intermolecular ones, which should play a more important role at longer times. In any case, the discrepancy is not large and we can state that the overall agreement is excellent regarding the structural properties as well as the dynamical features in a wide time range (the widest accessible by neutron scattering in this Q-range).

V. RESULTS

After the thorough validation of the simulated cell, we can take the advantages offered by simulations and calculate magnitudes not accessible by experiments, in particular, the correlations in real space. Let us consider first the self-part of the van Hove correlation function averaged over all the hydrogens in the sample, $G_s^{\mathrm{H}}(r,t)$. Figure 5 shows this function at three temperatures. We realize a qualitatively different behavior at different temperatures: At 280 K—well above T_g—the distribution continuously broadens and shifts toward larger distances with increasing time. These are typical signatures of a diffusive process as that involved in the structural α-relaxation. Contrarily, at 200 K, the most prominent feature in the distribution function is the development of a second peak centered at about 3 Å. This double-peak structure reveals an underlying localized process as, e.g., a jump

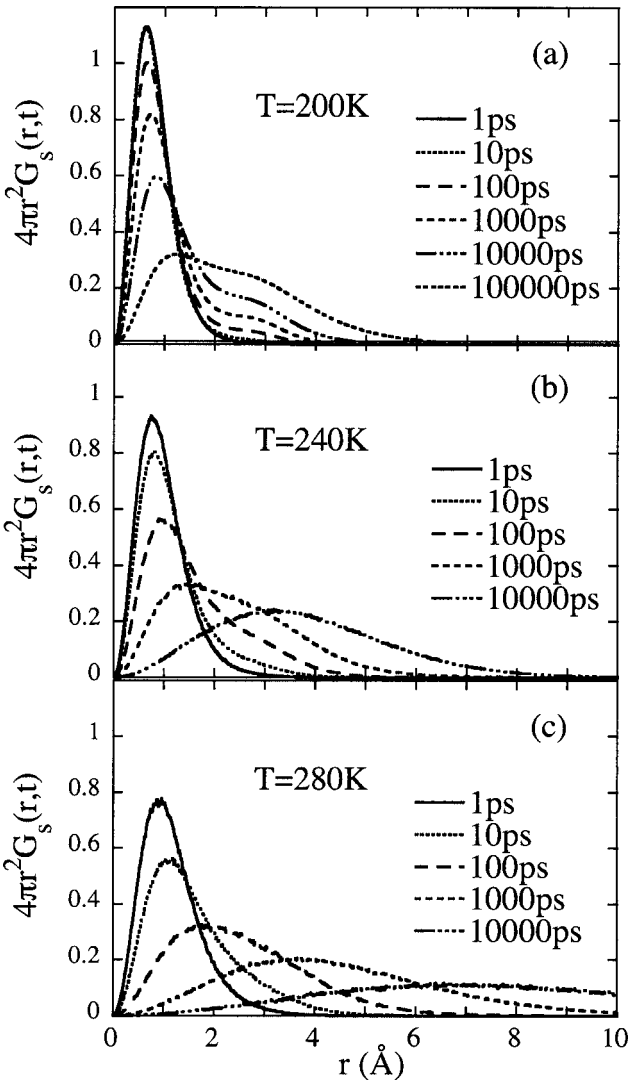

FIG. 5. Time evolution of the radial probability distribution function calculated for all hydrogens at three temperatures: (a) 200 K, (b) 240 K, and (c) 280 K and the times indicated.

between two positions separated by a distance $d\approx 2.5$ Å (roughly the distance between both peaks). At this temperature, the characteristic features of an incipient diffusion can be only envisaged at the long-time limit of the simulation window. The data at 240 K show an intermediate behavior; at 10 and 100 ps, the presence of localized processes is clear, and the role of the diffusion becomes important at rather short times (about 1 ns). A close inspection again of the 280 K data at times slightly slower than the microscopic regime, e.g., at 10 ps, reveals also a long tail in the distribution function which could be a hint of such local processes.

The occurrence of these local motions strongly influences the short-time region of the correlation functions and other related quantities, as, e.g., the mean squared displacement of the hydrogens $\langle r_{\mathrm{H}}^2(t)\rangle$. This function is displayed in Fig. 6(a) for all the temperatures studied. Again a distinct behavior is evident at high and low temperatures. At 280 K, the decaging mechanism takes place almost immediately after the microscopic regime (picosecond region). In contrast, at 200 K, the slope $\approx 1/2$ (expected limit for the decaging process towards the Rouse regime) is reached at rather long

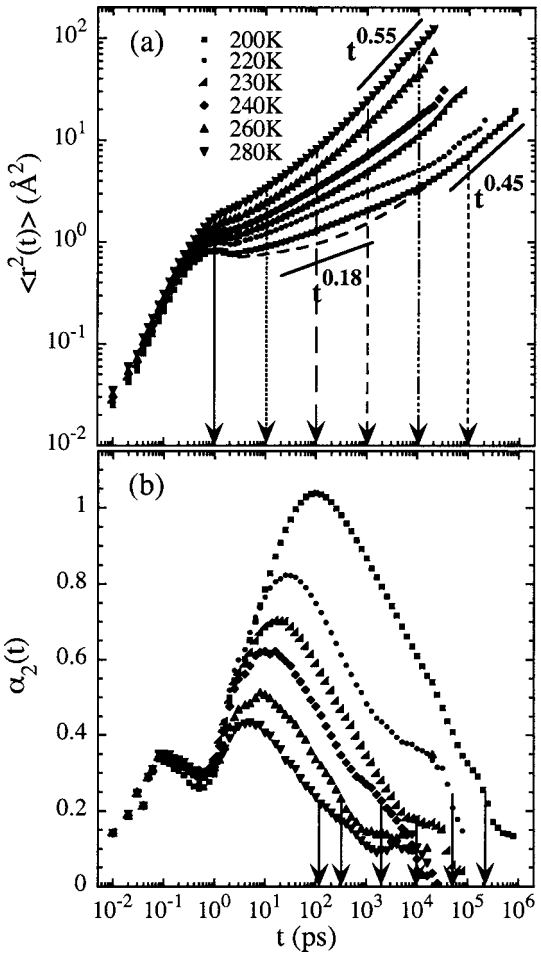

FIG. 6. (a) Mean squared displacement and (b) non-Gaussian parameter calculated for all the hydrogens in 1,4-PB at the different temperatures indicated. The vertical arrows in (a) indicate the times considered in Fig. 5. The dashed curve shows a diffusive-like contribution (sublinear affected by the fast microscopic decay) at 200 K. The solid lines indicate representative power laws. The vertical arrows in (b) mark the location of the structural relaxation time for each temperature.

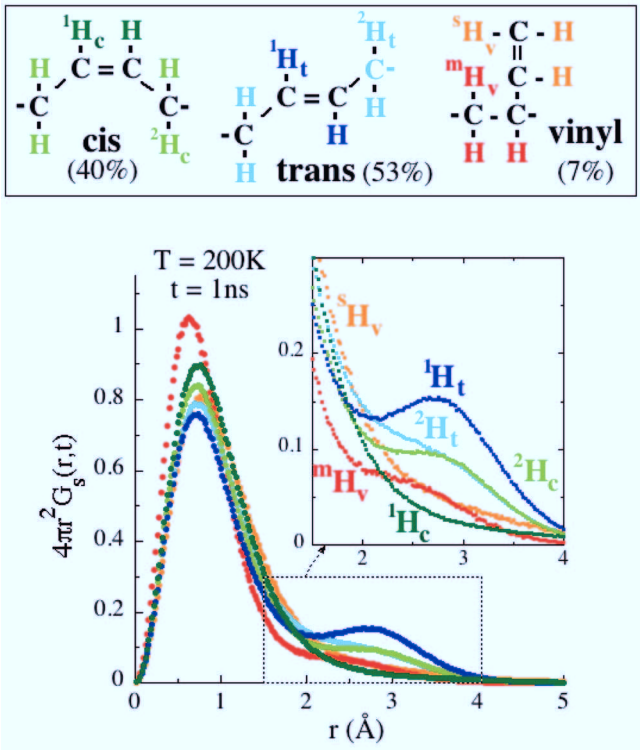

FIG. 7. (Color) Radial probability distribution function calculated at 200 K and $t=1$ ns for the different kinds of hydrogen in 1,4-PB. See in the panel above the schematic representation of the isomeric forms of PB monomers, illustrating with colors the nomenclature adopted for the different types of hydrogen.

times (beyond 10 ns). Interestingly enough, in the region between the microscopic and the final decaging dynamics, instead of the *a priori* expected plateau, we find a progressive increase of $\langle r_{\mathrm{H}}^2(t)\rangle$ (slope $\approx$0.2). This feature suggests an additional dynamical process occurring within the cage imposed by the neighboring molecules. This process is the local motion seen in $G_s^{\mathrm{H}}(r,t)$ (Fig. 5).

We note also the strong evolution of the non-Gaussian parameter $\alpha_2(t)$ with temperature [Fig. 6(b)]. In particular, at 200 K, the maximum reaches a very high value above 1. Its position (100 ps) is located in the time region where the first signatures of the local processes are visible [Fig. 5(a)]. Apparently, these local jumps are at the origin of the deviations from Gaussian behavior of $G_s(r,t)$, which smear out when the diffusive-like process plays a significant role.

It is worth noting that severe deviations from Gaussian behavior and unexpectedly slow increases of the hydrogen mobility in the region of $\approx$1–20 ps had been reported from the time of flight investigation of 1,4-PBh.[6] These observations support again the validity of the simulated cell. Moreover, the observed local jumps evident in the MD simulations provide an explanation of the time of flight results.

The simulations also allow to distinguish the motions of the different hydrogens in the sample. From an experimental point of view, this task in principle would be feasible by using selectively deuterated samples; however, in practice this is quite difficult to realize (see, e.g., Ref. 17), and of course impossible in real space. We have distinguished the following types of hydrogen: Meythyne hydrogens in *cis* [$^1\mathrm{H}_c$] or in *trans* unit [$^1\mathrm{H}_t$], methylene hydrogens in *cis* [$^2\mathrm{H}_c$] or *trans* unit [$^2\mathrm{H}_t$], and vinyl hydrogens bonded to main-chain carbons [$^m\mathrm{H}_v$] or in the side group [$^s\mathrm{H}_v$] (see Fig. 7 for the definitions). As can be seen in Fig. 7 for 200 K, an inspection of the self-part of the van Hove correlation function for each type of hydrogen reveals a strongly heterogeneous behavior: The jumps occur in a distinct manner depending on the kind of atom considered. The most visible feature is shown by $^1\mathrm{H}_t$, while $^1\mathrm{H}_c$ and $^s\mathrm{H}_v$ display—if any—a very weak signature for the same time. Such dynamic heterogeneity is also clearly reflected in the mean squared displacements and the $\alpha_2(t)$ parameters calculated for the different hydrogens (see Fig. 8). For example, the largest differences in the microscopic dynamics are found for the hydrogens in the vinyl groups: The extent of the motion within the cage for the side group hydrogens $^s\mathrm{H}_v$ doubles that of the main-chain hydrogens $^m\mathrm{H}_v$. Also the extremely high value of the $\alpha_2(t)$ parameter exhibited by $^s\mathrm{H}_v$ should be noted. Since the vinyl units amount to only 7% of the sample, we will focus on the hydrogens in the *cis* and *trans* units. In particular, we will emphasize the $^1\mathrm{H}_t$ and $^1\mathrm{H}_c$ atoms, which display the most diverse behavior. We can see that above $\approx$5 ps $^1\mathrm{H}_t$

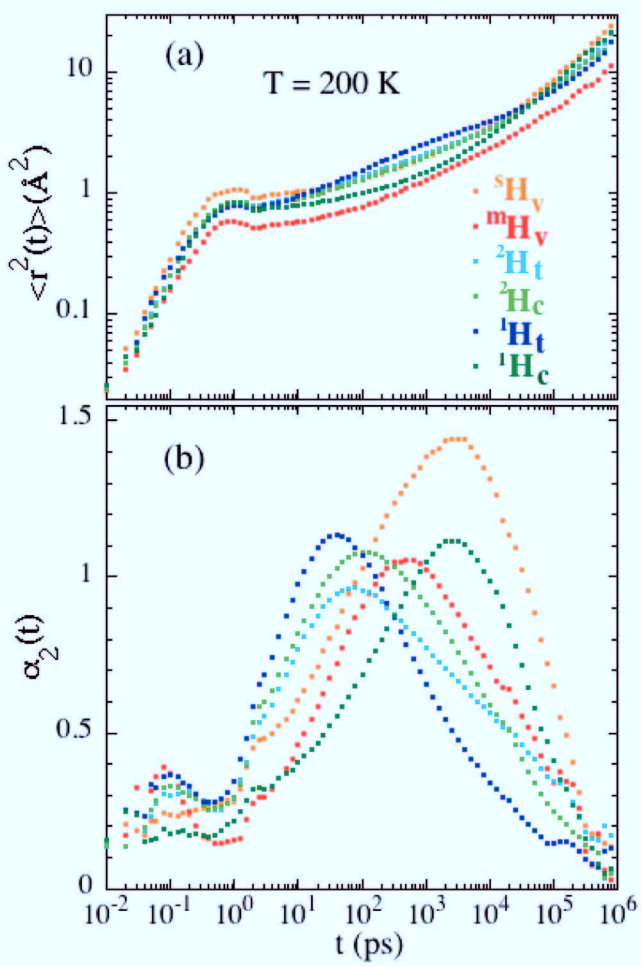

FIG. 8. (Color) (a) Mean squared displacement and (b) non-Gaussian parameter calculated for the different kinds of hydrogen in 1,4-PB at 200 K.

show a higher mobility than $^{1}H_c$, and the difference between the $\langle r^2(t)\rangle$ of both atoms continuously increases until the $^{1}H_c$ atoms initiate a faster dynamics at $\approx$1 ns; finally, at long times, the overall diffusion restores the homogeneity. We can also see that the positions of the maxima of $\alpha_2(t)$ differ by almost two decades in time for these two kinds of atoms.

Figure 9 displays the results at 280 K. In this case, the behavior is much more homogeneous, in particular, at longer times when diffusion is the overwhelming mechanism. However, in the 10 ps range, the contribution of local processes is still evident for the $^{1}H_t$ atoms.

VI. MODEL

We now consider a simple model capturing the essential features of the dynamics observed after the microscopic regime, i.e., the occurrence of local motions and diffusive-like processes. To describe the local process, we consider the hydrogen atom hopping over a jump distance d in an double well potential. In principle, this potential can be asymmetric with an asymmetry energy ΔE. Due to the disorder in the system, a distribution of hopping times reflecting the different environments is expected. This distribution is modeled

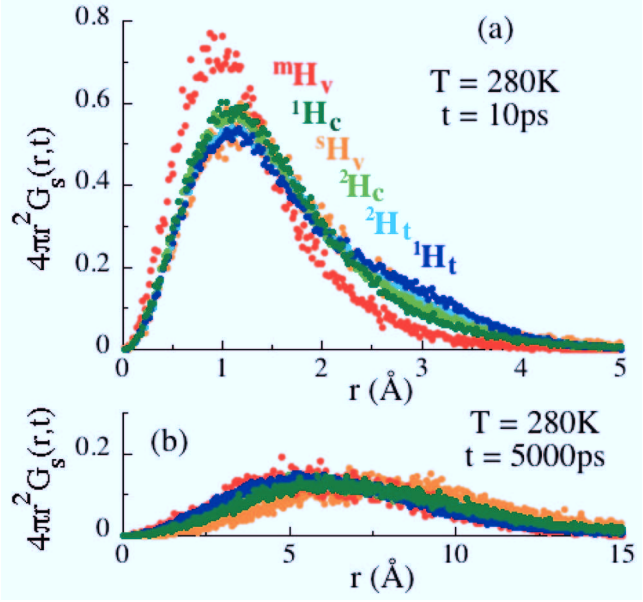

FIG. 9. (Color) Radial probability distribution function calculated at 280 K and (a) t=10 ps and (b) t=5 ns for the different kinds of hydrogen in 1,4-PB.

by a stretched exponential with a characteristic time $\tau_{\rm hop}$ and a stretching exponent $\beta_{\rm hop}$. The corresponding self-part of the van Hove correlation function reads

$$G_s^{\rm hop}(r,t) = [\eta_1^2 + \eta_2^2 + 2\eta_1\eta_2 e^{-(t/\tau_{\rm hop})^{\beta_{\rm hop}}}]\delta(r,t) + 2\eta_1\eta_2[1 - e^{-(t/\tau_{\rm hop})^{\beta_{\rm hop}}}]\delta(r-d,t), \quad (12)$$

with the thermal occupation factors $\eta_1=[1+\exp(-\Delta E/k_BT)]^{-1}$ and $\eta_2=\eta_1\exp(-\Delta E/k_BT)$. The time $\tau_{\rm hop}$ reflects the asymmetry of the potential as it is given by $1/\tau_{\rm hop}=\Gamma(1+\exp(\Delta E/k_BT))$, with Γ the characteristic frequency.

The atom undergoes also the diffusion process. In a first approximation, we assume the simultaneous occurrence of the two motions, which is expressed as the convolution of the corresponding van Hove correlation functions.[56] This implies the substitution of the $\delta(r,t)$ and $\delta(r-d,t)$ functions in Eq. (12) by the self-part of the van Hove correlation function of the diffusive process, $G_s^{\rm diff}(r,t)$ and $G_s^{\rm diff}(r-d,t)$.

$$G_s(r,t) = [\eta_1^2 + \eta_2^2 + 2\eta_1\eta_2 e^{-(t/\tau_{\rm hop})^{\beta_{\rm hop}}}]G_s^{\rm diff}(r,t) + 2\eta_1\eta_2[1 - e^{-(t/\tau_{\rm hop})^{\beta_{\rm hop}}}]G_s^{\rm diff}(r-d,t). \quad (13)$$

Previous works show (see, e.g., Refs. 49, 57, and 58) that the diffusive process involved in the structural relaxation is an anomalous diffusion where the mean squared displacement increases in a sublinear way with time, $\langle r^2(t)\rangle=6(Dt)^{\beta_{\rm diff}}$. The stretching exponent $\beta_{\rm diff}$ and the anomalous diffusion coefficient D are thus the characteristic parameters and $G_s^{\rm diff}(r,t)$ can be described by a Gaussian function [Eq. (4)] with $\alpha(t)=(Dt)^{-\beta_{\rm diff}}/4$. We note that the proper normalization of the Gaussian function centered at $r=d$ is given by

$$G_s^{\text{Gauss}}(r-d,t)=\frac{e^{-\alpha(t)(r-d)^2}}{2\pi\left\{\frac{d}{\alpha(t)}e^{-\alpha(t)d^2}+\sqrt{2\pi}\left[\frac{d^2}{\sqrt{2\alpha(t)}}+\frac{1}{\sqrt{(2\alpha(t))^3}}\right][1+\text{erf}(d\alpha(t))]\right\}}. \quad (14)$$

With this, we have established all the ingredients for our model. Finally, in order to reproduce the data, we have also to take into account the effect of the microscopic dynamics at timescales above ≈1 ps, where we will apply our model. In this regime, the microscopic dynamics within the cage has reached its stationary state leading to a constant value of the associated mean squared displacement. In the self-correlation function $G_s(r,t)$, this leads to a time-independent broadening. In a first approximation, we describe this effect by a Gaussian function [Eq. (4)] of constant width given by the mean squared displacement within the cage, $\alpha(t)=3/(4\langle u^2\rangle)$ (u is the displacement in each of the three dimensions) and incorporate this additional constant broadening in $G_s^{\text{diff}}(r,t)$. Then, our final model function is given by Eq. (13), where $G_s^{\text{diff}}(r,t)$ and $G_s^{\text{diff}}(r-d,t)$ are Gaussian [Eqs. (4) and (14)] with

$$\alpha(t)=\frac{1}{4(Dt)^{-\beta_{\text{diff}}}}+\frac{3}{4\langle u^2\rangle}. \quad (15)$$

We now apply the model to the methyne hydrogens in both 1,4 units, ^1H_t and ^1H_c, which show the most diverse behavior. For each of these atoms, as a first step, we describe the initial correlation function at $t=1$ ps, where neither the local process nor the diffusion is yet contributing to the self-part of the van Hove correlation function. The goal is to obtain the value of $\langle u^2\rangle$ related to the microscopic dynamics which would be kept constant for all fits at later times. Since a single Gaussian is not able to properly account for the data, we use a sum of two initial Gaussians with different widths (i.e., different values of $\langle u^2\rangle$). In this simple way, we account for the deviations from Gaussian behavior of the microscopic contribution. We note that such deviations were, in fact, expected in view of the nonvanishing values of the $\alpha_2(t\approx 1\text{ ps})$ parameter [see, e.g., Fig. 6(b)]. As shown in Fig. 10, we observe very similar results for the Gaussian widths for both kinds of atoms. This figure also compares the results to experimental values from the decay of elastic scattering in the time of flight data.[6] The Gaussian with the smaller $\langle u^2\rangle$ approaches the extrapolation of the low-temperature behavior, while the other component shows much higher values of $\langle u^2\rangle$, indicating strong anharmonicities. This component could be related to the so called "fast process" which was subject of a strong debate in the literature (see, e.g., Refs. 6 and 59–68). The experimental data lie in between the two sets of values and coincide rather well with their average. We note that the comparison is semiquantitative, since (i) the contributions of all hydrogens should be taken into account for a direct comparison and (ii) part of the contribution to the experimentally determined values of $\langle u^2\rangle$ is due to the dynamics above 1 ps; therefore, for the highest temperatures the experimental values could be slightly overestimated. However, this comparison is very satisfactory and supports again the reliability of the simulations, now regarding the microscopic regime.

For the subsequent application of the model, we consider thus the addition of the corresponding two Gaussians with the fixed values of $\langle u^2\rangle$ as obtained from the above described procedure. For each temperature, the values of the parameters [β_{hop}, τ_{hop}, d, ΔE, D, and β_{diff}] are obtained from a simultaneous fit of the model to data equispaced in log t. For the lowest temperature (200 K), the time range considered was restricted to $t\leqslant 30$ ns (see below). The solid lines in Fig. 11 present the descriptions obtained for the considered atoms at different times and temperatures. As can be appreciated, over the full temperature and time range considered, this very simple model describes the simulation data very accurately.

Figure 12 shows that for the case of the *trans* atoms the model also provides an excellent description of the time evolution of the mean squared displacement and the non-Gaussian parameter for the different temperatures.

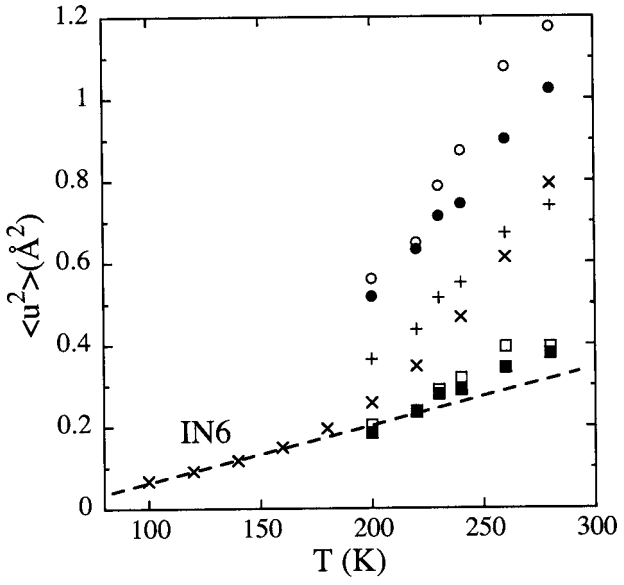

FIG. 10. Temperature dependence of the mean squared displacement of the two Gaussian functions describing the initial distribution in the MD simulations. Empty symbols correspond to ^1H_c atoms and full symbols to ^1H_t. The pluses are the average over the two components and over the kind of hydrogen weighted by their relative abundance in the sample. The crosses represent the values experimentally obtained from time of flight measurements (Ref. 6). The dashed line shows the low-temperature behavior and its extrapolation.

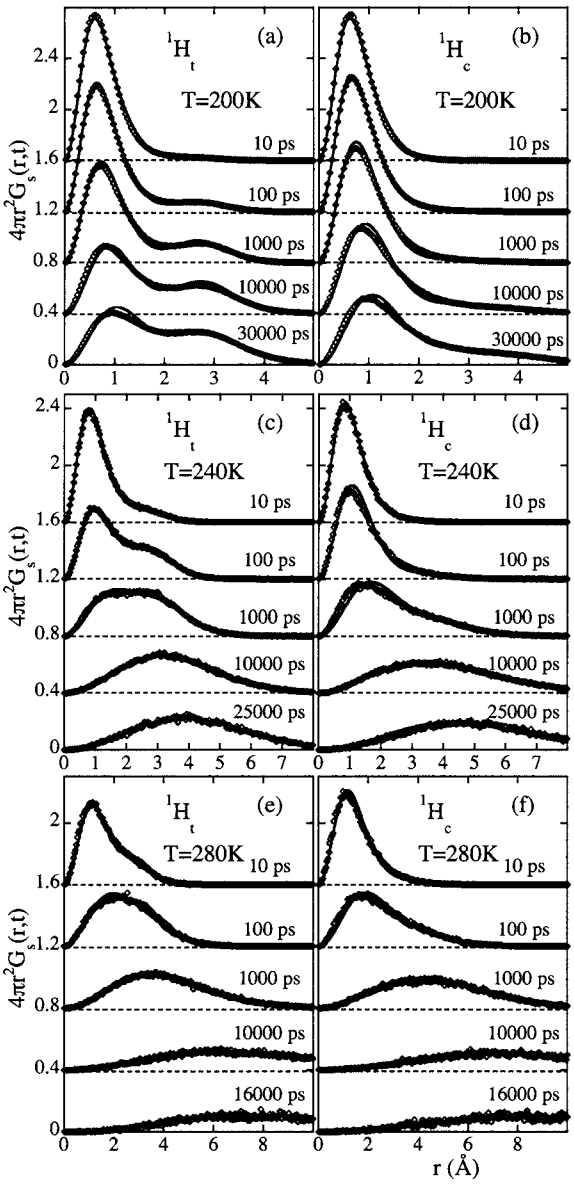

FIG. 11. Radial probability distribution function calculated at [(a) and (b)] 200 K, [(c) and (d)] 240 K and [(e) and (f)] 280 K at the different times indicated for [(a), (c), and (e)] ^1H_t and [(b), (d), and (f)] ^1H_c. For clarity, the origins are shifted to the levels displayed by the horizontal dotted lines. The solid lines show the description obtained by the proposed model (see text).

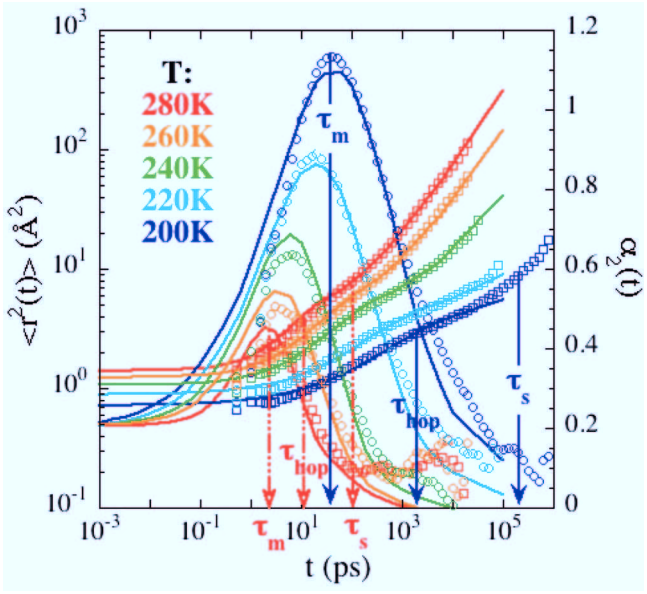

FIG. 12. (Color) Mean squared displacement (squares) and non-Gaussian parameter (circles) calculated for the ^1H_t atoms at the different temperatures indicated. The lines are the descriptions obtained by the model proposed. The vertical arrows indicate the locations of τ_m [maximum of $\alpha_2(t)$], τ_{hop}, and the structural relaxation time τ_s for 200 K (solid) and 280 K (dashed-dotted).

VII. DISCUSSION

A. Hopping process

We start discussing the results on the jump process. Its characterization is easier for the case of the methyne hydrogens in the trans units, ^1H_t, since their hopping timescale is faster and well separated from the diffusion. Focusing first on these atoms, a well-defined jump distance can be deduced which slightly decreases with increasing temperature from $d_t(200\ \mathrm{K})=2.47$ Å to $d_t(280\ \mathrm{K})=2.34$ Å. The asymmetry of the potential is found to be rather small for all the temperatures investigated ($\Delta E_t \leqslant k_B T$). Figure 13 shows the temperature dependence of the parameters characterizing the distribution functions of relaxation times. The distribution continuously narrows with increasing temperature, which could be a signature of an underlying distribution of potential barriers. The characteristic time follows a nearly perfect Arrhenius-type dependence with an activation energy of $E_a^t=0.30$ eV. In the case of the ^1H_c atoms, the signatures of the hopping processes are much more subtle. Assuming a single jump distance, it is not possible to describe the simulation results. However, a Gaussian distribution of jump lengths allows a good description of the data, as can be appreciated in the right panels of Fig. 11. The resulting average jump distance $\langle d_c \rangle=2.6$ Å hardly depends on temperature, while the values of the width of the distribution function σ increase from 1 Å at 200 K to 1.3 Å at 280 K. This distribution reflects the more hindered motion of ^1H_c compared to its *trans* counterpart. On the other hand, the asymmetry of the potential is negligible also for ^1H_c. Concerning the distributions of hopping times, they show similar widths as for the ^1H_t; however, the timescales are sensibly longer than those exhibited by the *trans* atoms—in fact, as shown in Fig. 13(b), they are rather close to the structural relaxation time—and can be described by an Arrhenius law with $E_a^c=0.38$ eV.

In the following, we compare the features of these hopping processes with the main processes identified either experimentally or by other simulations (Fig. 14). Considering first the simulation results, we note that in the investigated temperature range, the timescales found for the jump process of the ^1H_t atoms show values intermediate between those reported by Gee and Boyd[26] for the torsional autocorrelation function of the β- and α-bonds (see Fig. 14). Thereby the bond adjacent to the double bond is named α while the more distant bond in between two α-bonds is named β. At high temperature τ_{hop}^t is close to that of the *α-trans* time while at low temperature it approaches the *β-trans* values. Nevertheless given the geometry of the double bond in the *trans* conformation, we would have expected that the quoted *α-trans*

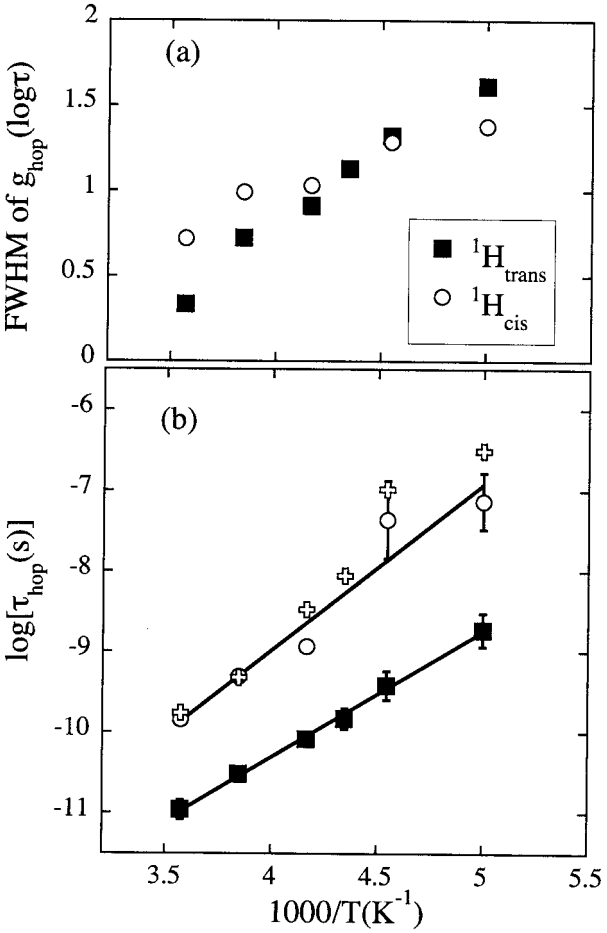

FIG. 13. Temperature dependence of the parameters characterizing the jumps of ^1H_t (full squares) and ^1H_c (empty circles): (a) Full width at half maximum of the distribution function of relaxation times and (b) characteristic times. In (b), the solid lines are fitted to Arrhenius laws and the structural relaxation time deduced from the simulations (Table I) is also shown for comparison (pluses).

dynamics agrees broadly with the ^1H_t motions. The jump distance of $d_t \approx 2.4$ Å corresponds well to conformational jumps of the ^1H_t atom which according to Gee and Boyd should be a cooperative motion involving the single bonds on both sides of the double bond in *trans* conformation.[28] For the ^1H_c atoms, τ_{hop}^c is longer than the values corresponding to the β-bond for such units,[26] but approaches them very closely at high temperatures.

Hopping processes of ^1H_t were also identified in the MD simulation of 1,4-*trans* polybutadiene reported by Kim and Mattice.[28] They interpret the ^1H_t motion as due to the reorientation of a CH═CH bond via cooperative counter-rotation at its two flanking CH–CH_2 bonds. This mechanism allows the double bond to hop without disturbing other monomers along the chain. Thereby each hydrogen atom on the double bond (^1H_t) rallies between two virtually fixed locations because the counter-rotation is fast compared to any other intramolecular relaxation modes and the relaxation of the surrounding medium as well. This explains why jump motions of ^1H_t manifest as a distinct hopping peak in the van Hove correlation function. To check the hopping process of ^1H_t in a model-independent way, we have calculated the module of the displacement vector $|\vec{r}(0)-\vec{r}(t)|$ of the different

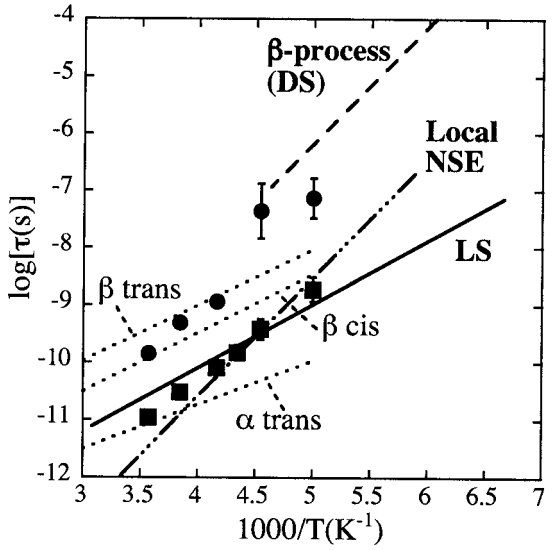

FIG. 14. Map of secondary and local processes identified for 1,4-PB. Experimental results: Arrhenius fit of the DS β-relaxation (Ref. 3) (dashed line), the process observed by light scattering (Ref. 7) (solid line), and the local process identified by NSE (Refs. 2 and 3) (dashed-dotted line). Simulation results: Timescales deduced in this work for the hopping processes of the ^1H_t (squares) and ^1H_c atoms (circles) and reported by Gee and Boyd (Ref. 26) for torsional autocorrelation functions (dotted lines, see text).

^1H_t in our simulation cell. Figure 15 shows the distribution of $|\vec{r}(0)-\vec{r}(t)|$ for one representative ^1H_t. This distribution has been calculated by subtracting the average value of $|\vec{r}(0)-\vec{r}(t)|$ and therefore it is centered at 0. The distribution shows a double peak and almost equally populated structure, confirming the hopping mechanism. Kim and Mattice[28] considered the counter-rotation mechanism crucial to observe a defined hopping peak in $G_s(r,t)$. They suggest that in the case of *cis*-PB the hopping peak would be more visible for methylene hydrogen (^2H_c) instead of for methyne ^1H_c, via counter-rotation across a rotable CH_2–CH_2 bond. This is confirmed by our simulations (see Fig. 7). Unfortunately, the

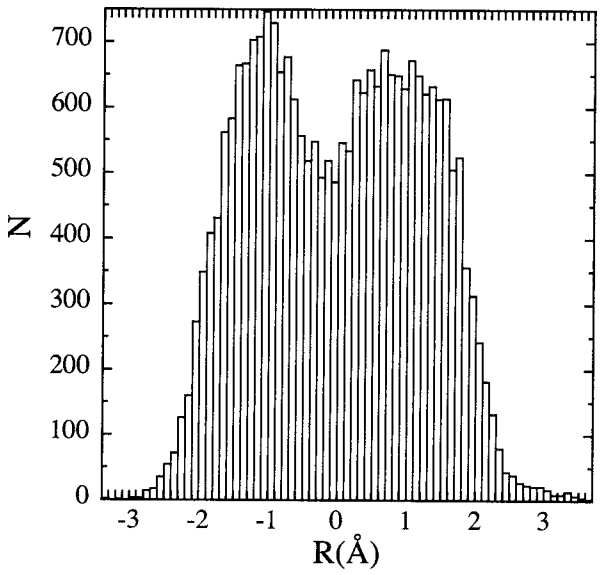

FIG. 15. Distribution of the position of a given ^1H_t with respect to its average value along the simulation run. The temperature considered is 200 K.

hopping times are not calculated in Ref. 28; therefore, a quantitative comparison to our results is not possible.

The α- and β-relaxations have also been investigated by MD simulations in a united-atom model of 1,4-PB by Smith and Bedrov.[36] They conclude that the β-relaxation process can be associated with large-scale conformational motions corresponding to all or nearly all dihedrals visiting each conformational state. Although in principle this view can be compatible with our results, a direct comparison is not possible due to the different magnitudes computed and, in particular, because in the 1,4-PB model used in Ref. 36 the intramolecular barriers for dihedral transition of the polymer backbone were reduced by a factor of 4 in relation to the original 1,4-PB model.

Moving to the processes determined experimentally, we note from Fig. 14 that the times corresponding to the *trans* atoms perfectly match the experimental findings from the damping of Brillouin modes.[7,8] Thus, depolarized light scattering seems to be sensitive to this kind of fast local motions involving the *trans* units. On the other hand, the hopping time of the *cis* atoms is much closer to the timescale of the secondary β-relaxation observed by DS. This is very reasonable, since it is the *cis* unit that carries the electric dipole moment in this sample. This similarity suggests the relation between the local motions involved in the dielectric β-relaxation and the distributed hopping processes found in these simulations.

Let us now consider the comparison with the NSE study of 1,4-PBd addressing the question of the merging of the α and β-processes.[3] Those experimental data were interpreted in terms of statistically independent local and diffusive processes, like here. A simple model was proposed for the local process which in a first incoherent approximation delivered a jump length of the atoms of about 1.5 Å. Further considerations based on possible rotations of *cis* and *trans* units led to a scenario where the local processes observed could be interpreted as rotational jumps of the chain building blocks. Independently of the geometry assumed for the local motions, their characteristic timescale showed an activation energy very close to that of the β-relaxation as obtained by DS (0.41 eV), an observation that suggested the identification of those motions with the origin of the dielectric relaxation. However, the absolute values of the times deduced from the NSE experiments were more than two orders of magnitude faster than the dielectric ones, preventing a clear link between the two processes. As we will show, our results are perfectly consistent with the scenario proposed in that work and allow clarification of open questions. Figure 14 evidences that the local process characterized in the NSE study is the rapid motion involving the *trans* units. In the fully deuterated sample employed, NSE is of course sensitive to all atoms and naturally the dynamics of the *cis* units should also be observed. However, the hopping process undergone by the *cis* units is much slower than that of the *trans* atoms, and, in fact, occurs in a timescale very close to that of the structural relaxation. At temperatures below and close to the merging—where the timescale of the local process was determined—the NSE technique explores the fastest part of the second decay of the dynamic structure factor after the microscopic regime. The dynamics accessed there is dominated by the fastest local processes, which are those of the *trans* units. This explains the small values obtained for the characteristic times in Ref. 51. Regarding the hopping distance reported in that work (1.5 Å), it may seem to be in disagreement with the values close to 2.4 Å found here for ^1H_t. However, this apparent discrepancy can be perfectly rationalized in noting that the distance involved in the simulations corresponds to the jump of hydrogen atoms, while NSE is equally sensitive to all the atoms (carbons and deuterons). Since in the rotational jumps the motional amplitude of carbons should be smaller than that of hydrogen, the observation of an effectively smaller jump distance can be expected.

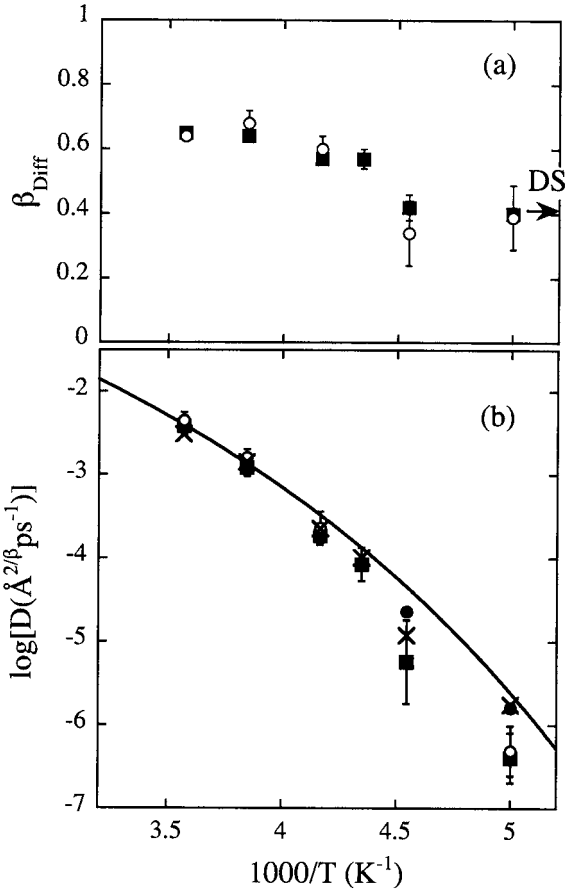

FIG. 16. Temperature dependence of the parameters characterizing the diffusion of ^1H_t (full squares) and ^1H_c (empty circles): (a) Shape parameter and (b) anomalous diffusion coefficient. For 200 K, the application of the model was restricted to $t \leq 30$ ns. In (b), the full circles are obtained from the fit of the model at $t \geq 30$ ns, and the crosses are determined from the long-time behavior of the main-chain carbons in the vinyl units; the solid line shows the expected dependence from the study of the structural relaxation time.

The present study has thus allowed placing the experimental observations regarding local or secondary processes in 1,4-PB into a context. Let us now move to the diffusive process.

B. Diffusive process

We first note that the obtained values of the anomalous diffusion coefficient D as well as of the stretching exponent β_{diff} are almost identical for ^1H_t and ^1H_c (see Fig. 16). This result is consistent with our scenario, since the underlying

mechanism of the diffusive motion should be the same for all atoms in the sample. For the stretching exponent β_{diff}, we observe an increase with increasing temperature, from about 0.4 at 200 and 220 K to ≈0.65 at 280 K [see Fig. 16(a)]. In order to compare these to other results, we recall that the stretching exponent describes the stretched exponential decay of the measured relaxation function. Considering first the DS,[3] a value of 0.41 was determined for the shape parameter of the α-process in the temperature range $T_g \leqslant T \leqslant 200$ K, where the α- and β-relaxations are well separated.[3] The agreement with our results at low temperatures (200 K for the simulated sample should be equivalent to about 215 K for the real sample) is good. Regarding the comparison to the NSE data on the structural relaxation, from the above discussion in the validation section, and taking into account the results of Fig. 2(a), we can say that the NSE β values are slightly smaller than β_{diff} at the equivalent temperatures, but in any case compatible within the uncertainties. Furthermore, they show a similar general tendency to increase with increasing temperature.

Now let us focus on the anomalous diffusion coefficient. Figure 16(b) displays its temperature dependence together with the expected behavior from the analysis of the structural relaxation times [D should be inversely proportional to Eq. (11) with $B=1404.5$ and $T_o=113$ K]. As can be seen in this figure, the agreement is good at high temperatures, while for 220 and 200 K the diffusion deduced for the protons at times shorter than 30 ns is slower than expected from the decay of the interchain correlations at the first structure factor peak.

We have already mentioned that for 200 K the model was successfully applied, but only up to times below 30 ns. The reason is that at this temperature it is not possible to simultaneously describe the data below and above $t \approx 30$ ns with the same parameters for the diffusive process. The value obtained for D from the fit at $t \leqslant 30$ ns is about four times smaller than that deduced from longer times, which, in fact, should be better determined, since there the diffusion is the dominant mechanism. If we consider these long-time values as indicative for the true translational diffusion, then we arrive at the full circles in Fig. 16(b), which follow nearly perfectly the expected temperature law. For the higher temperatures (280, 260, and 240 K) such a problem does not occur and we achieve a very good overall description.

We can deduce an independent approximation to the diffusion coefficient from the long-time increase of the mean squared displacement of the main-chain carbon of the vinyl groups. We choose these particular atoms because for them the hopping processes could be expected to be least probable and they would undergo almost pure diffusion. The such obtained diffusion coefficient (crosses) again follows very nicely the temperature dependence of the structural relaxation time. Thus, in the low-temperature range investigated the diffusion process seems to be more intrincate than just a simple continuous motion and at 200 K a change in the diffusion mechanism could be guessed in the time region of ≈30 ns. In fact, as we will show later (Fig. 18), at smaller Q's the self-intermediate scattering function $F_s(Q,t)$ of $^1\text{H}_t$ and $^1\text{H}_c$ displays an acceleration in the long-time region after

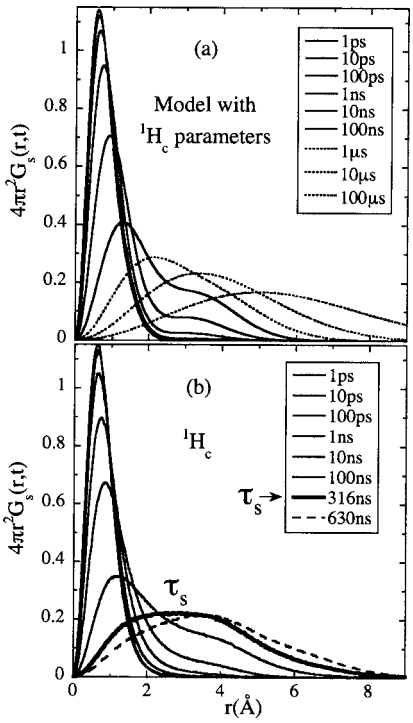

FIG. 17. Radial probability distribution function at 200 K at the times indicated: (a) Obtained with the fit parameters of the $^1\text{H}_c$ atoms and (b) calculated from simulations for $^1\text{H}_c$ atoms.

the *cis*-relaxation time ($\tau^c_{\text{hop}} \approx 70$ ns). This change in the time dependence of $F_s(Q,t)$ suggests the existence of a delayed diffusion process—the onset of the long-time translational diffusion appears to be coupled with the completion of the *cis*-group relaxation.

For long times, the self-part of the van Hove correlation functions of $^1\text{H}_t$ and $^1\text{H}_c$ is shown in Fig. 17. As can be appreciated, in the neighborhood of the *cis*-relaxation time, the correlators also display some anomalies. At $t \approx \tau^c_{\text{hop}}$, the height of the distribution in the region of the second maximum becomes bigger than in the first maximum [see panel (b)], an effect which cannot be reproduced by our model [see panel (a)], which assumes continuous diffusion. This feature suggests some mechanism which leads to a change in the population of the two maxima. As can be seen in the figure, the setting of such mechanism produces a notable increase of the main position of the distribution with respect to the expected one from the model with the parameters deduced from the short time regime. Though we do not have a molecular explanation for this effect, we think that it might indicate a triggering mechanism which is at the basis of the delayed long-time translational diffusion. This mechanism appears to be related to the *cis*-conformational transitions. Furthermore, we note the closeness of the τ^c_{hop} and τ_s time-scales.

C. Non-Gaussian behavior

As can be appreciated in Fig. 12, our model provides an excellent description of the mean squared displacement and the non-Gaussian parameter of the $^1\text{H}_t$ atoms. The high values of $\alpha_2(t)$ at low temperatures as well as its evolution with temperature are very well reproduced. We realize that this

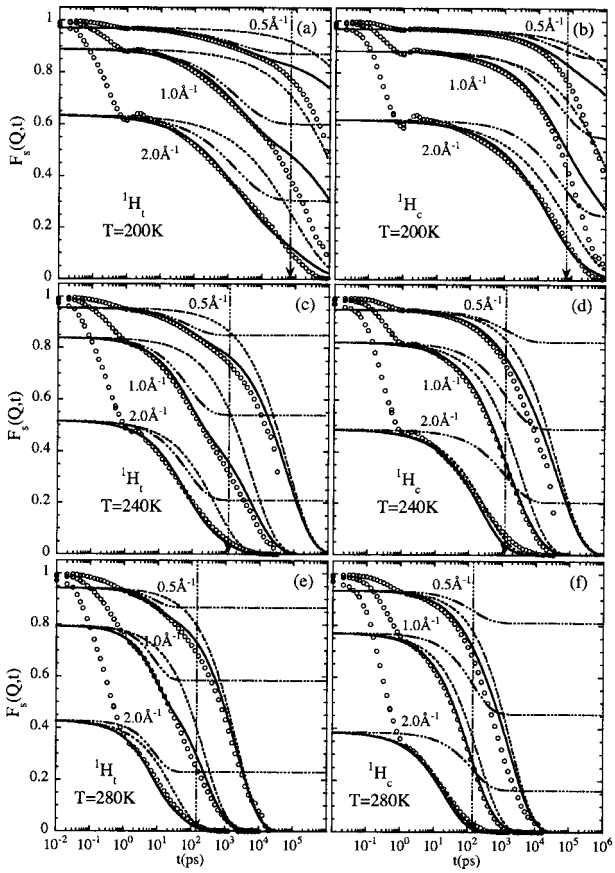

FIG. 18. Intermediate scattering function calculated at [(a) and (b)] 200 K [(c) and (d)] 240 K and [(e) and (f)] 280 K for Q=0.5 Å^{-1}, Q=1 Å^{-1} and 2 Å^{-1} for [(a), (c), and (e)] ^{1}H$_t$ and [(b), (d), and (f)] ^{1}H$_c$. The solid lines show the curves obtained through Eq. (16) with the parameters obtained from the real space analysis (see text). The dotted and dashed-dotted lines represent the contributions of the diffusion and hopping processes, respectively. The vertical arrows show the values of τ_{hop}^{c}.

model also captures a feature of 1,4-PB which is usually not present in other systems: In 1,4-PB, the timescale of the maximum of $\alpha_2(t)$, which we will denote τ_m, is much shorter than the structural relaxation time τ_s and does not scale with it. This is clearly shown in Fig. 12, where we have indicated for 280 and 200 K the locations of τ_m, τ_{hop}^{t}, and τ_s. For 200 K, there are more than three decades between τ_m and τ_s; this difference is reduced to less than two decades for 280 K. Similar results also hold for the van Hove correlation function averaged for all the hydrogens in the sample [see Fig. 6(b)]. When commenting Figs. 6(b) and 5, we noticed that the $\alpha_2(t)$ parameter reaches its maximum in the very early stages of the hopping process. This can also be realized from Fig. 12: τ_m is located in the region where the mean squared displacement begins to increase after the microscopic dynamics, even much earlier than the characteristic timescale for the hopping process τ_{hop}. In fact, since the diffusive contribution is considered Gaussian, in the framework of this model the peak of $\alpha_2(t)$ is entirely due to the hopping process. The Gaussian diffusion smears the long-time flank of this peak as it approaches the microscopic region with increasing temperature. This means that the diffusive process restores the Gaussianity. Our main conclusion is the essential observation that the deviations from Gaussian behavior appear and have maximum visibility when the particle leaves its initial localization, independently of the mechanism leading to it—a diffusive-like jump process or a hopping process like in this case. In systems with no internal degrees of freedom, the delocalization can only take place by the structural relaxation; in systems displaying rich local dynamics such as polymers, initial delocalization may take place first through the localized motions leading to secondary relaxations.

D. Visibility of local processes in *Q*-space

1. Self-motions

Scattering experiments always access the reciprocal space. Fourier transformation of our model function yields the intermediate scattering function for self-motion,

$$F_s(Q,t) = \exp\left(-\frac{Q^2\langle u^2\rangle}{3}\right)\exp[-Q^2(Dt)^{\beta_{\mathrm{diff}}}]\left\{\eta_1^2+\eta_2^2 + 2\eta_1\eta_2\frac{\sin(Qd)}{Qd} + 2\eta_1\eta_2\left(1-\frac{\sin(Qd)}{Qd}\right) \times\exp\left[-\left(\frac{t}{\tau_{\mathrm{hop}}}\right)^{\beta_{\mathrm{hop}}}\right]\right\}. \quad (16)$$

For both ^{1}H$_t$ and ^{1}H$_c$, Fig. 18 displays the prediction of Eq. (16) for several Q-values at three temperatures and compares them to the simulated structure factors. Our simple model reveals an overall very good description of the MD data in the range of its applicability (above the microscopic region, $t \gtrsim 1$ ps), with the above commented exception of the long-time region ($t \gtrsim 30$ ns) at 200 K. There, we can see an acceleration of the decay with respect to the expected behavior from the shorter time description of the correlation function. Above we have associated this behavior with a delay of the long-time translational diffusion due to a coupling with the *cis*-group relaxation.

Within its limitations, the model thus depicts all major dynamic features of the system. We can observe that with decreasing temperature the shape of $F_s(Q,t)$ becomes strongly stretched, corroborating the recent united-atom simulations of 1,4-PB (Refs. 31 and 35) for $S(Q,t)$. It is worth emphasizing that, while in real space the local jump dynamics can easily be distinguished from the anomalous diffusion (mainly for ^{1}H$_t$), in Fourier space no evidence for a separate process other than the anomalous stretching at low temperature appears.

The dotted lines in Fig. 18 present the predictions for the anomalous diffusion neglecting the hopping term. At all Q-values, strong deviations between the simulated structure factor and the predicted diffusion structure factor are evident. This holds even for low-Q-values, where common wisdom would not suspect any influence from the local motions. The effect is of course more visible at lower temperatures, where the timescales for diffusion and hopping differ more. This is a direct consequence of the model. A low-Q and short-time expansion of Eq. (16),

$$F_s(Q,t) \approx 1 - \left[\frac{1}{3}\eta_1\eta_2 d^2\left(\frac{t}{\tau_{\text{hop}}}\right)^{\beta_{\text{hop}}} + \frac{\langle u^2\rangle}{3} + (Dt)^{\beta_{\text{diff}}}\right]Q^2, \quad (17)$$

shows that both the hopping and the diffusion terms appear as coefficients for Q^2. It follows that for fast hopping processes well separated in time from the overall anomalous diffusion, the hopping contribution will dominate even at small Q.

Measurements in this time regime will be in particular sensitive to the local dynamics and will reveal temperature dependencies different from that of the α-process. Thus in a system with important internal degrees of freedom displaying a dynamics well separated from the overall motional processes, the dynamics of such degrees of freedom have an important impact on the self-correlation function even in the low-Q regime. The observations that at low-Q $F_s^{\text{H}}(Q,t)$ in polyisobutylene,[69] poly(vinyl chloride),[70] and PMMA (Ref. 53) give rise to a weaker temperature dependence than that of the structural relaxation most likely can be rationalized in a similar way and seem to indicate a general trend.

2. Collective dynamics

In general, the calculation of the coherent version of any model function is not easy, since it involves the correlations of all possible atomic pairs. In our case, taking into account the structural and dynamic complexities of the sample, achieving a good description of the dynamic structure factor based on the simple model proposed is far from realistic. Nevertheless, we can use our simulation results to check whether they support predictions based on the previously used model for the coherent scattering function of the local motions involved in the secondary relaxation.[2,3] In the simplest version of that model, the amplitude of the quasielastic contribution to the structure factor was approximated by its incoherent counterpart, which for a jump between two equivalent sites separated by a distance d is given by $A^{\text{hop}}(Q,d)=[1-\sin(Qd)/(Qd)]/2$. Taking into account that by NSE we access the structure factor normalized by its static value $S(Q)$, the relative quasielastic amplitude of the local process is given by $A^{\text{hop}}(Q,d)/S(Q)$. Figure 19 shows with the dashed line this prediction, using $d=1.5$ Å as deduced in those works.[2,3] As we can see, with this "incoherent" approximation, we understand the selectivity of NSE to the structural relaxation at the first peak, since there the contributions from local processes should be strongly suppressed. In addition, a surprising feature emerges in the Q-range *below* the first maximum of $S(Q)$: A rather strong quasielastic contribution from the local processes is predicted where intuitively these processes should not appreciably contribute to the decay of the dynamic structure factor. This prediction has never been checked experimentally. In the following, we search for a signature in our simulated data.

We consider 200 K, where $^1\text{H}_t$ hopping and the structural relaxation are most separated: $\tau_{\text{hop}}^t=2$ ns and $\tau_s^t=308$ ns, i.e., they differ by more than two orders of magnitude. At a time slightly slower than τ_{hop}^t, e.g., $t=5$ ns, the decay of the dynamic structure factor due to these hopping processes would be more or less complete, while the structural relaxation contribution should still be rather weak [see the incoherent function in Fig. 18(a)]. Therefore, $S(Q,t=5\text{ ns})$ could be considered a first approximation for the coherent elastic contribution characteristic for hopping. However, the correlations have partially decayed before in the microscopic regime ($t\lesssim 1$ ps). Thus, in a similar way as the NSE data were corrected for the DWF in the fitting procedure in Refs. 2 and 3, we have taken into account the renormalization to this amplitude when we have calculated from the simulations the relative quasielastic contribution of the local process to the normalized structure factor. The result is shown in Fig. 19. As we can appreciate, the agreement with the prediction of the simple model proposed in Refs. 2 and 3 (dotted line) is noteworthy, especially in the Q-range below 1.7 Å^{-1} and close to the second maximum of $S(Q)$. We note that the NSE measurements at 2.7 Å^{-1} were the most important to determine the geometry of the hopping processes in those works. There, the model matches simulated data with rather high accuracy. On the other hand, interestingly, the simulated data also reproduce the increase of the quasielastic contribution at low-Q-values below the first peak of $S(Q)$ and thus strongly support the renormalization procedure previously proposed. New NSE experiments are foreseen in order to experimentally prove this notable quasielastic contribution of the local processes to the structure factor at low-Q-values.

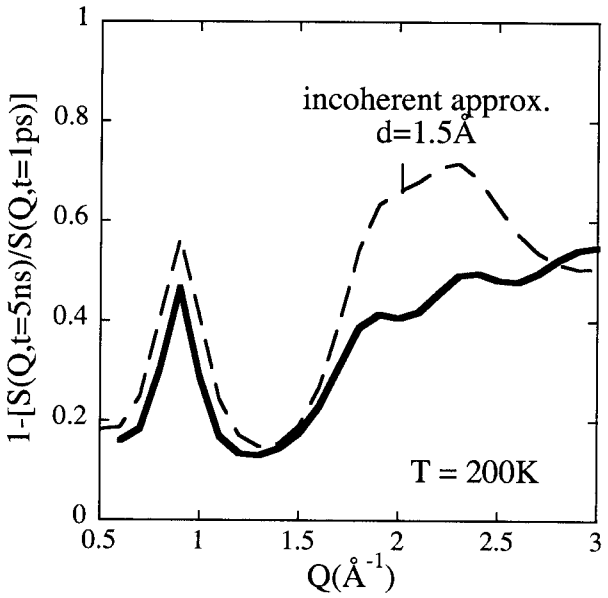

FIG. 19. Fraction of the dynamic structure factor relaxed at 5 ns with respect to the value at 1 ps (solid line). The dashed line shows the prediction of the simple model proposed in Refs. 2 and 3 with a jump length of 1.5 Å for the relative quasielastic contribution.

E. Further approaches

We have seen that the local processes affect the correlation functions and related magnitudes in the timescale between the microscopic regime and the structural relaxation. What is the impact of these motions on the application of the

current theories for glass-forming dynamics to polymer data? In fact, we note that the region of maximum visibility of the localized motions is just located in the time window where the MCT for the glass transition[37] predicts the occurrence of *its* β-process, which *a priori* is not related to the *Johari–Goldstein* β-process or other secondary processes. The β-regime of the MCT is dominated by the "cage"effect imposed by the surrounding neighbors. Then, the question arises whether the MCT can be applied to 1,4-PB and what is the influence of the local process in the results of such analysis.

In a recent work,[38] it has been shown that, at least formally, MCT can be applied to the results of the fully atomistic MD simulations presented here, and its main predictions are fulfilled. Apparently, the MCT analysis reflects the presence of the local conformational changes through the large value deduced for the exponent parameter λ. Similarly high values were also obtained in the MCT analysis of the united-atom model used by Paul *et al.*[35] As discussed in Ref. 38, values of λ approaching 1 point to a situation close to a MCT higher-order transition ($\lambda=1$).[71–73] Features associated with such transitions have been recently reported for attractive colloids[74] and a series of systems showing strong confinement effects.[75–77] The origin of the observed anomalous relaxation features is attributed to the presence of several competing mechanisms for dynamic arrest—steric repulsion and reversible bond formation in Ref. 74, bulk-like caging and confinement in Refs. 75–77. In the case of the $\alpha\beta$-region of real polymers, it has been proposed[38] that there also exist two active and simultaneous mechanisms leading to dynamic arrest: (i) Packing of intermolecular character and present in all glass-forming systems; (ii) barriers for conformational changes ("β-like"), of intramolecular origin, which are specific of real macromolecular systems.

VIII. SUMMARY AND CONCLUSIONS

From simple inspection of the simulation results and their comparison to experimental data, we have made the following observations:

- The simulated cell represents very well the dynamical features of 1,4-PB at $t \gtrsim 1$ ps if a shift of about 15 K in the glass transition is assumed.
- A real space analysis allows establishing the occurrence of (i) hopping processes, most evident, in the methyne-*trans* hydrogen and (ii) diffusive contributions.
- The dynamics is heterogeneous: The different atoms distinguished move in a different way.
- We observe a suppression of the contributions of local motions in the neighborhood of the first static structure factor peak and an enhancement of such hopping processes below this peak, as predicted in earlier works.[2,3]
- Non-Gaussian effects are detected at very earlier times, when the decaging from the initial cage takes place. For the *trans* atoms, the origin of such deviations can be attributed to the hopping motion within the cage, not to the decaging due to the structural relaxation.
- The visibility of the local motions is maximum at timescales where the MCT β-process is expected to take place.

In this work we have applied the phenomenological model proposed in Ref. 23 to the simulation data in the whole temperature range investigated. This model assumes simultaneous occurrence of hopping and diffusive motions, and is applicable after the microscopic regime ($t \gtrsim 1$ ps). We can draw the following conclusions.

- The model captures very nicely the evolution of the probability distribution function in real space, with the restrictions of times above $\approx$30 ns for the 200 K data.
- We obtain an extremely accurate description for the *trans* atoms. There, the timescales of hopping and diffusion are well separated and the jump distance is well defined. These motions can be interpreted in terms of fast counterrotations of *trans*-units as proposed by Kim and Mattice.[28]
- The *cis* atoms show an underlying distribution of jump distances and a hopping timescale very close to the structural relaxation time.
- In the α-β merging regime around 200–220 K, a coupling of diffusion and *cis*-relaxation seems to take place with effect of accelerating the translational diffusion at $t \gtrsim 30$ ns.
- We have been able to put the experimental observations into a context, relating the DS β-process to the local motions of the *cis* units and the processes identified by light scattering and NSE with the hopping *trans* process.
- The statistically independence of hopping and diffusion at atomic level is clearly fulfilled for the *trans* hydrogens.
- The local processes appreciably contribute to the decay of the intermediate incoherent scattering function of the hydrogens also in the low-Q range. This might lead to an apparent weaker temperature dependence of the neutron scattering results with respect to the expected dependence dictated by the structural relaxation.

Finally, we refer to the work[38] regarding the applicability of the MCT to 1,4-PB data. There, it was shown that it is possible to apply this theory, though a new scenario is suggested based on the existence of two mechanisms for dynamic arrest.

ACKNOWLEDGMENTS

This research project has been supported by the European Commission NoE SoftComp, Contract No. NMP3-CT-2004-502235. A.A., F.A., and J.C. acknowledge support from Project Nos. MAT2007-63681 and IT-436-07 (G.V.) and the Spanish Ministerio de Educacion y Ciencia (Grant No. CSD2006-53). "Donostia International Physics Center"

is also acknowledged. A.N. acknowledges the FPI grant of the Spanish Ministry of Science and Technology.

[1] A. Hofmann, A. Alegría, J. Colmenero, L. Willner, E. Buscaglia, and N. Hadjichristidis, Macromolecules **29**, 129 (1996).
[2] A. Arbe, U. Buchenau, L. Willner, D. Richter, B. Farago, and J. Colmenero, Phys. Rev. Lett. **76**, 1872 (1996).
[3] A. Arbe, D. Richter, J. Colmenero, and B. Farago, Phys. Rev. E **54**, 3853 (1996).
[4] S. A. Lusceac, C. Gainaru, M. Vogel, C. Koplin, P. Medick, and E. A. Rössler, Macromolecules **38**, 5625 (2005).
[5] G. C. Berry and T. G. Fox, Adv. Polym. Sci. **5**, 261 (1968).
[6] R. Zorn, G. B. McKenna, L. Willner, and D. Richter, Macromolecules **28**, 8552 (1995).
[7] A. Aouadi, M. J. Lebon, C. Dreyfus, B. Strube, W. Steffen, A. Patkowski, and R. M. Pick, J. Phys.: Condens. Matter **9**, 3803 (1997).
[8] Y. Ding, V. N. Novikov, and A. P. Sokolov, J. Polym. Sci., Part B: Polym. Phys. **42**, 994 (2004).
[9] A. P. Sokolov, U. Buchenau, D. Richter, C. Masciovecchio, F. Sette, A. Mermet, D. Fioretto, G. Ruocco, L. Willner, and B. Frick, Phys. Rev. E **60**, R2464 (1996).
[10] D. Richter, B. Frick, and B. Farago, Phys. Rev. Lett. **61**, 2465 (1988).
[11] B. Frick, D. Richter, and Cl. Ritter, Europhys. Lett. **9**, 557 (1989).
[12] B. Frick, B. Farago, and D. Richter, Phys. Rev. Lett. **64**, 2921 (1990).
[13] D. Richter, R. Zorn, B. Farago, B. Frick, and L. J. Fetters, Phys. Rev. Lett. **68**, 71 (1992).
[14] R. Zorn, D. Richter, B. Frick, and B. Farago, Physica A **201**, 52 (1993).
[15] U. Buchenau, A. Wischnewski, D. Richter, and B. Frick, Phys. Rev. Lett. **77**, 4035 (1996).
[16] R. Zorn, T. Kanaya, T. Kawaguchi, D. Richter, and K. Kaji, J. Chem. Phys. **105**, 1189 (1996).
[17] S. Kahle, L. Willner, M. Monkenbusch, D. Richter, A. Arbe, J. Colmenero, and B. Frick, Appl. Phys. A: Mater. Sci. Process. **74**, 371 (2002).
[18] R. Zorn, Phys. Rev. B **55**, 6249 (1997).
[19] B. Frick, C. Alba-Simionesco, K. H. Andersen, and L. Willner, Phys. Rev. E **67**, 051801 (2003).
[20] B. Frick, G. Dosseh, A. Cailliaux, and C. Alba-Simionesco, Chem. Phys. **292**, 311 (2003).
[21] A. Cailliaux, C. Alba-Simionesco, B. Frick, L. Willner, and I. Goncharenko, Phys. Rev. E **67**, 010802 (2003).
[22] A. Narros, A. Arbe, F. Alvarez, J. Colmenero, R. Zorn, W. Schweika, and D. Richter, Macromolecules **38**, 9847 (2005).
[23] J. Colmenero, A. Arbe, F. Alvarez, A. Narros, M. Monkenbusch, and D. Richter, Europhys. Lett. **71**, 262 (2005).
[24] Y. Li and W. L. Mattice, Macromolecules **25**, 4942 (1992).
[25] E.-G. Kim, S. Misra, and W. L. Mattice, Macromolecules **26**, 3432 (1993).
[26] R. H. Gee and R. H. Boyd, J. Chem. Phys. **101**, 8028 (1994).
[27] G. D. Smith, W. Paul, M. Monkenbusch, L. Willner, D. Richter, X. H. Qiu, and M. D. Ediger, Macromolecules **32**, 8857 (1999).
[28] E. G. Kim and W. M. Mattice, J. Chem. Phys. **117**, 2389 (2002).
[29] O. Okada and H. Furuya, Polymer **43**, 971 (2002).
[30] P. Gestoso, E. Nicol, M. Doxastakis, and D. N. Theodorou, Macromolecules **36**, 6925 (2003).
[31] G. D. Smith, D. Bedrov, and W. Paul, J. Chem. Phys. **121**, 4961 (2004).
[32] D. Bedrov, G. D. Smith, and W. Paul, Phys. Rev. E **70**, 011804 (2004).
[33] J. Colmenero, F. Alvarez, A. Narros, A. Arbe, M. Monkenbusch, D. Richter, and B. Farago, *CP708, Slow Dynamics in Complex Systems: Third International Symposium*, 2004, edited by M. Tokuyama and I. Oppenheim, AIP, New York, p. 655.
[34] G. Tsolou, V. G. Mavrantzas, and D. N. Theodorou, Macromolecules **38**, 1478 (2005).
[35] W. Paul, D. Bedrov, and G. D. Smith, Phys. Rev. E **74**, 021501 (2006).
[36] G. D. Smith and D. Bedrov, J. Polym. Sci., Part B: Polym. Phys. **45**, 627 (2007).
[37] W. Götze, in *Liquids, Freezing, Glass Transition*, edited by J. P. Hansen, D. Levesque, and J. Zinn-Justin (North-Holland, Amsterdam, 1991), p. 287.
[38] J. Colmenero, A. Narros, F. Alvarez, A. Arbe, and A. J. Moreno, J. Phys.: Condens. Matter **19**, 205127 (2007).
[39] H. Sun, J. Comput. Chem. **15**, 752 (1994); H. Sun, S. J. Mumby, J. R. Maple, and A. T. Hagler, J. Am. Chem. Soc. **116**, 2978 (1994); H. Sun, Macromolecules **28**, 701 (1995); **26**, 5924 (1994); H. Sun, S. J. Mumby, J. R. Maple, and A. T. Hagler, J. Phys. Chem. **99**, 5873 (1995).
[40] See, for example: H. Sun, J. Phys. Chem. B **102**, 7338 (1998); http://www.accelrys.com/doc
[41] D. N. Theodorou and U. W. Suter, Macromolecules **18**, 1467 (1985).
[42] D. N. Theodorou and U. W. Suter, Macromolecules **19**, 379 (1986).
[43] T. Springer, *Quasielastic Neutron Scattering for the Investigation of Diffusive Motions in Solids, Liquids*, Springer Tracts in Modern Physics Vol. 64 (Springer-Verlag, Berlin, 1972).
[44] A. Rahman, K. S. Singwi, and A. Sjölander, Phys. Rev. **126**, 986 (1962).
[45] S. W. Lovesey, *Theory of Neutron Scattering from Condensed Matter* (Clarendon, Oxford, 1984).
[46] M. Bée, *Quasielastic Neutron Scattering* (Adam Hilger, Bristol, 1988).
[47] G. L. Squires, *Introducction to the Theory of Thermal Neutron Scattering* (Dover, New York, 1996).
[48] F. Mezei, *Neutron Spin Echo*, Lecture Notes in Physics Vol. 28 (Springer-Verlag, Heidelberg, 1980).
[49] D. Richter, M. Monkenbusch, A. Arbe, and J. Colmenero, *Neutron Spin Echo Investigations on Polymer Dynamics*, Advances in Polymer Science Vol. 174 (Springer, Berlin, 2005).
[50] J. Colmenero, A. Arbe, D. Richter, B. Farago, and M. Monkenbusch, in *Neutron Spin Echo Spectroscopy. Basics, Trends and Applications*, edited by F. Mezei, C. Pappas, and T. Gutberlet (Springer, Berlin, 2003), p. 268.
[51] A. Arbe, J. Colmenero, F. Alvarez, M. Monkenbusch, D. Richter, B. Farago, and B. Frick, Phys. Rev. E **67**, 051802 (2003).
[52] A. Narros, F. Alvarez, A. Arbe, J. Colmenero, D. Richter, and B. Farago, J. Chem. Phys. **121**, 3282 (2004).
[53] A.-C. Genix, A. Arbe, F. Alvarez, J. Colmenero, B. Farago, A. Wischnewski, and D. Richter, Macromolecules **39**, 6260 (2006).
[54] S. Mossa, R. Di Leonardo, G. Ruocco, and M. Sampoli, Phys. Rev. E **62**, 612 (2000).
[55] A. Soldera and Y. Grohens, Polymer **45**, 1307 (2004).
[56] The assumption of simultaneous occurrence of statistically independent processes was also made in a previous work on the dynamics of 1,4-PB in the $\alpha\beta$-merging region (Ref. 3) based in the ansatz proposed by Williams [see, e.g., G. Williams, Adv. Polym. Sci. **33**, 60 (1979)]. This ansatz was also successfully applied to results on several systems [F. Alvarez, A. Hoffman, A. Alegría, and J. Colmenero, J. Chem. Phys. **105**, 432 (1996); R. Bergman, F. Alvarez, A. Alegría, and J. Colmenero, *ibid.* **109**, 7546 (1998); A. Kudlik, C. Tschirwitz, T. Blochowitz, S. Benkhof, and E. Rössler, J. Non-Cryst. Solids **235–237**, 406 (1998); D. Gómez, A. Alegría, A. Arbe, and J. Colmenero, Macromolecules **287**, 503 (2001)].
[57] J. Colmenero, A. Alegría, A. Arbe, and B. Frick, Phys. Rev. Lett. **69**, 478 (1992).
[58] A. Arbe, J. Colmenero, M. Monkenbusch, and D. Richter, Phys. Rev. Lett. **81**, 590 (1998).
[59] B. Frick and D. Richter, Science **267**, 1939 (1995).
[60] F. Fujara and W. Petry, Europhys. Lett. **4**, 921 (1987).
[61] W. Knaak, F. Mezei, and B. Farago, Europhys. Lett. **7**, 529 (1988).
[62] W. Doster, S. Cusack, and W. Petry, Phys. Rev. Lett. **65**, 1080 (1990).
[63] E. Bartsch, O. Debus, F. Fujara, M. Kiebel, H. Sillescu, and W. Petry, Ber. Bunsenges. Phys. Chem. **95**, 1146 (1991).
[64] B. Frick, R. Zorn, D. Richter, and B. Farago, J. Non-Cryst. Solids **131–133**, 169 (1991).
[65] T. Kanaya, K. Kaji, and K. Inoue, Macromolecules **24**, 1826 (1991).
[66] J. Wuttke, M. Kiebel, E. Bartsch, F. Fujara, W. Petry, and H. Sillescu, Z. Phys. B: Condens. Matter **91**, 357 (1993).
[67] J. Colmenero, A. Arbe, and A. Alegría, Phys. Rev. Lett. **71**, 2603 (1993).
[68] J. Colmenero and A. Arbe, Phys. Rev. B **57**, 13508 (1998).
[69] B. Farago, A. Arbe, J. Colmenero, R. Faust, U. Buchenau, and D. Richter, Phys. Rev. E **65**, 051803 (2002).
[70] A. Arbe, A. Moral, A. Alegría, J. Colmenero, W. Pyckhout-Hintzen, D. Richter, B. Farago, and B. Frick, J. Chem. Phys. **117**, 1336 (2002).
[71] W. Götze and R. Haussmann, Z. Phys. B: Condens. Matter **72**, 403 (1988).
[72] M. Sperl, Phys. Rev. E **68**, 031405 (2003).
[73] V. Krakoviack, Phys. Rev. Lett. **94**, 065703 (2005).
[74] F. Sciortino, P. Tartaglia, and E. Zaccarelli, Phys. Rev. Lett. **91**, 268301 (2003).
[75] A. J. Moreno and J. Colmenero, J. Chem. Phys. **124**, 184906 (2006).
[76] A. J. Moreno and J. Colmenero, Phys. Rev. E **74**, 021409 (2006).
[77] A. J. Moreno and J. Colmenero, J. Chem. Phys. **125**, 164507 (2006).